

Scalable and Efficient Continual Learning from Demonstration via a Hypernetwork-generated Stable Dynamics Model

Sayantan Auddy*, Jakob Hollenstein*, Matteo Saveriano†, Antonio Rodríguez-Sánchez*, Justus Piater*‡

* Department of Computer Science, University of Innsbruck, Austria

† Department of Industrial Engineering, University of Trento, Italy

‡ Digital Science Center (DiSC), University of Innsbruck, Austria

Abstract—Learning from demonstration (LfD) provides an efficient way to train robots. The learned motions should be convergent and stable, but to be truly effective in the real world, LfD-capable robots should also be able to remember multiple motion skills. Existing stable-LfD approaches lack the capability of multi-skill retention. Although recent work on continual-LfD has shown that hypernetwork-generated neural ordinary differential equation solvers (NODE) can learn multiple LfD tasks sequentially, this approach lacks stability guarantees. We propose an approach for *stable continual-LfD* in which a hypernetwork generates *two* networks: a *trajectory learning* dynamics model, and a *trajectory stabilizing* Lyapunov function. The introduction of stability generates convergent trajectories, but more importantly it also greatly improves continual learning performance, especially in the size-efficient *chunked hypernetworks*. With our approach, a single hypernetwork learns stable trajectories of the robot’s end-effector position and orientation simultaneously, and does so continually for a sequence of real-world LfD tasks without retraining on past demonstrations. We also propose *stochastic hypernetwork regularization* with a *single* randomly sampled regularization term, which reduces the cumulative training time cost for N tasks from $\mathcal{O}(N^2)$ to $\mathcal{O}(N)$ without any loss in performance on real-world tasks. We empirically evaluate our approach on the popular LASA dataset, on high-dimensional extensions of LASA (including up to 32 dimensions) to assess scalability, and on a novel extended robotic task dataset (RoboTasks9) to assess real-world performance. In trajectory error metrics, stability metrics and continual learning metrics our approach performs favorably, compared to other baselines. Our open-source code and datasets are available at <https://github.com/sayantanauddy/clfd-snode>¹.

Index Terms—Learning from demonstration, continual learning, hypernetworks.

I. INTRODUCTION

Learning from demonstration (LfD) is a natural way for humans to impart movement skills to robots. Robots trained with LfD are required to not only reproduce the motions demonstrated by the human user, but also to guarantee the stability of the produced motion [1]. Methods employed for LfD must be able to make sure that the robot’s trajectory does not diverge, and that the robot does not assume unsafe configurations during its motion. Accordingly, the focus of recent LfD techniques [2]–[6] has been on ensuring that these required stability and convergence properties are satisfied.

However, these LfD methods focus on learning only a single motion skill. Consequently, to learn a new skill the robot must be retrained from scratch and the previously learned skill is forgotten. Recent work in *continual LfD* [7] has shown that a system of *neural ordinary differential equation solvers* (NODEs) [8] and *hypernetworks* [9], [10] can continually learn and remember a sequence of motion skills without the need of retraining on past demonstrations. However, this approach has limitations such as lack of stability of the learned vector field, degrading performance for long task sequences, and increase in hypernetwork training time for each additional task, resulting in an overall training time cost of $\mathcal{O}(N^2)$. In the current paper we address these limitations which are critical for a robot in the real world.

We propose a novel continual-LfD system in which a hypernetwork generates the parameters of our proposed time-dependent *stable* NODE (*sNODE*) that is composed of *two* neural networks: (i) a network that represents a nominal dynamics model, and (ii) an additional network that parameterizes a *Lyapunov function* that is responsible for ensuring the stability of the predicted trajectories.

Our proposed continual-LfD system is able to learn and remember long sequences of trajectory learning tasks without storing or retraining on the data of past tasks. It produces stable, non-divergent trajectory predictions that eliminate the possibility of robot movements that are dangerous for humans in the vicinity of the robot or for the robot itself. Most importantly, we show that the introduction of stability leads to much improved continual learning performance compared to the non-stable alternative. This improvement is most prominent for *chunked* hypernetworks [7], smaller hypernetworks that produce the parameters of the target networks in smaller segments called *chunks*. With our proposed approach, these limited capacity hypernetworks are able to remember a long sequence of tasks, even for high-dimensional trajectory-learning tasks. In experiments involving real-world tasks, we propose a single model that can predict both the position and orientation of the robot’s end-effector simultaneously. In contrast to using separate models for position and orientation [7], our approach roughly halves the number of required model parameters without compromising on performance. We propose a stochastic regularization approach for hypernetworks in which a *single* randomly sampled regularization term is added to the

Corresponding author: sayantan.auddy@uibk.ac.at

¹This paper is currently under peer review.

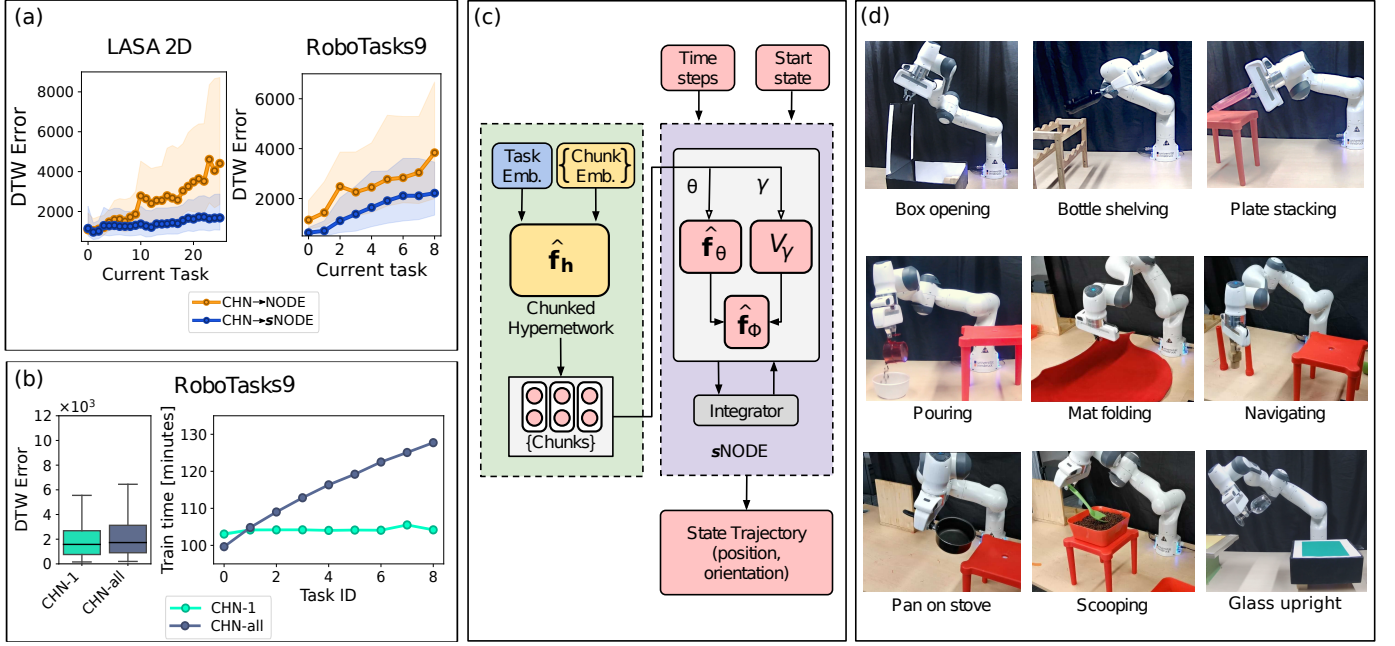


Fig. 1. Overview of key results and our proposed approach. (a) Continual learning from demonstration with stable NODEs generated by a chunked hypernetwork (CHN→sNODE) outperforms NODE-based continual learning (CHN→NODE) by a wide margin (details in Sec. VI). (b) Stochastic regularization with a single regularization term (CHN-1) leads to a CHN→sNODE model that performs as well as the fully regularized model (CHN-all) on real-world tasks but reduces the training cost of N tasks from $\mathcal{O}(N^2)$ to $\mathcal{O}(N)$ (details in Sec. VI). (c) Architecture of a CHN→sNODE model: a chunked hypernetwork (CHN) \hat{f}_h generates the parameters $\phi = \{\theta, \gamma\}$ of a stable NODE (sNODE) \hat{f}_ϕ , comprising a nominal dynamics model \hat{f}_θ and a Lyapunov function V_γ . Task-specific learned parameters are shown in ■, regularized (task-independent) learned parameters are shown in ■, and non-trainable inputs/outputs are shown in ■ (details in Sec. IV). (d) Illustrations of the nine real-world tasks of our proposed RoboTasks9 dataset. The last 5 tasks are introduced in this paper (details in Sec. V). With our proposed approach, all tasks can be learned in a continual manner with a single hypernetwork model without retraining on past demonstrations, with minimal forgetting, and with stability in the predicted trajectories.

optimization objective instead of adding a regularization term for each past task. With this approach, the cumulative training cost is reduced from $\mathcal{O}(N^2)$ to $\mathcal{O}(N)$ in the number of tasks N , without any impact on performance in real-world tasks.

We perform experiments on the popular LASA trajectory learning dataset [11] that contains 26 tasks [7] of 2-dimensional trajectories. To evaluate the scalability of our approach to higher dimensions, we create high-dimensional analogues of the LASA dataset. We combine multiple tasks from the original LASA dataset to create new datasets of 8-, 16-, and 32-dimensional trajectories. Each of these new datasets contain 10 tasks each. We add 5 new tasks to the *RoboTasks* dataset [7], creating a new dataset *RoboTasks9* containing 9 real-world LfD tasks. For all datasets (LASA 2D, LASA 8D, LASA 16D, LASA 32D, and RoboTasks9), we evaluate our hypernetwork→sNODE models against all major groups of continual learning methods (*replay*, *dynamic architectures*, and *regularization*) [12], as well as against the models using NODE proposed in [7]. We report quantitative metrics for the predicted trajectories, as well as for the continual learning performance. We also report stability metrics. Additionally, we evaluate our approach qualitatively on a Franka Emika Panda robot in the real world. An overview of our approach and key results are shown in Fig. 1. Our open-source code and datasets can be found at <https://github.com/sayantanaudhy/clfd-snode>.

Our contributions can be summarized as follows:

- We propose an approach for *stable, continual* learning from demonstration with hypernetworks and sNODE that

not only remembers multiple trajectory learning tasks and produces stable trajectories, but also improves the continual learning performance of the system compared to the non-stable alternative.

- We propose a time-dependent sNODE model that predicts more accurate trajectories than the time-independent model.
- We propose a single hypernetwork→sNODE model that learns multiple tasks continually and predicts position and orientation trajectories simultaneously for real-world tasks.
- We introduce a form of stochastic hypernetwork regularization with a *single* randomly sampled regularization term that reduces the cumulative training cost for N tasks from $\mathcal{O}(N^2)$ to $\mathcal{O}(N)$ without loss of performance on real-world tasks.
- We create high-dimensional versions of the LASA dataset, and extend the RoboTasks dataset [7] by adding 5 new real-world tasks to create RoboTasks9.

II. RELATED WORK

Learning from demonstration (LfD) is a robot learning methodology where a robot learns manipulation skills from human demonstrations. LfD is also referred to as *programming by demonstration* or *imitation learning* [13], [14]. The demonstrations may be provided by different means, including kinesthetic teaching (a human physically guides the robot to perform a motion task [14]–[17]), and tele-operation (the demonstrations

are provided by humans while operating a joystick-controlled robot). Learning directly from videos of humans or other robots performing manipulation tasks has also been investigated [18]. LfD is valuable for tasks that are difficult to program explicitly or learn from scratch, allowing robots to bootstrap from human expertise and adapt to various situations in complex domains. Different learning approaches, including supervised learning [19], [20], constrained optimization [21], reinforcement learning [22], and inverse reinforcement learning [23] have been utilized for LfD. In addition to Euclidean space, LfD in non-Euclidean spaces such as Riemannian manifolds is also a topic of current research [24], [25].

Similar to [7], we focus on *trajectory-based* learning, which is a subfield of LfD. Trajectory-based learning methods either fit probability distributions to the observed data with *generative models* [2], [3], [11], [26], or fit a discriminative model to the training data using function approximators such as neural networks [6], [27]. The observed demonstrations can either be used to learn a *static-mapping* between the time and desired state of the robot, or to learn a dynamics model that can predict the desired velocity of the robot from its current state (*dynamic mapping*). The mapping between robot states and velocities forms a vector field, and many different approaches have been proposed that ensure that the vector field is stable and converges to a desired target [2], [4]–[6]. Among methods that employ neural networks, Uraïn et al. [2] use normalizing flows to learn stable vector fields from demonstrations, and Manek and Kolter [6] learn stable vector fields by jointly learning a nominal dynamics model and a parameterized *Lyapunov* function.

Despite the maturity of research in trajectory-based LfD, the predominant focus of most approaches [2], [6] is on acquiring a single skill. This necessitates training a new model each time a new skill is to be learned. In contrast, our focus is on continually learning a sequence of LfD tasks. In [7], *Neural Ordinary Differential Equation solvers* (NODEs [8]) generated by Hypernetworks [9], [10] are employed for learning several LfD skills continually with a single model. However, NODEs lack stability guarantees, which may result in divergent trajectory predictions. In this paper, we propose *stable, continual-LfD*. We convert the previously mentioned dynamics model of Manek and Kolter [6] into a time-dependent dynamics model (which we refer to as *stable NODE* (*sNODE*)) that predicts more accurate trajectories, and generate the two constituent networks of this *sNODE* with a hypernetwork. Compared to [7], our present approach enables the learning of multiple tasks such that the predicted trajectories are always stable. Crucially, the introduction of stability leads to better continual learning performance, as we discuss later.

Continual Learning (CL) is a promising way for embodied agents like robots to gradually assimilate knowledge without needing to be preprogrammed to handle all possible future tasks *a priori*. Popular CL strategies include dynamically increasing the parameter size of a model [28], caching and replaying exemplars of training data from past tasks [29], using generative replay to generate pseudo-data of past tasks [30], or regularizing trainable parameters with additional constraints [31]–[33] to

avoid catastrophic forgetting [12].

Compared to the vast amount of research dedicated to image classification tasks [12], [34], only a relatively small number of papers focus on continual robot learning. The necessity of CL for robotics was identified in early work [35], where CL was applied to simple navigation and find-and-fetch tasks. More recently, Churamani et al. [36], [37] use CL to adapt the perception and behavior models of social robots to the changing behaviors of humans for more personalized human-robot interaction. Liu et al. [38] propose an approach based on Gradient Episodic Memory [39] for continual learning of robot navigation tasks. Trinh et al. [40] use regularization-based continual learning approaches such as Elastic Weight Consolidation [31] and Synaptic Intelligence [32] to adapt the dynamics model of an industrial robot to ever changing conditions. Sarabakha et al. [41] evaluate several continual learning methods such as Experience Replay [42], Learning without Forgetting [43], Average Gradient Episodic Memory [44], and an online version of Elastic Weight Consolidation [31], [45] for continually training mobile ground and aerial robots. Gao et al. [18] use deep generative replay [30] for generating pseudo-training data of past tasks that is interleaved with the current task’s demonstrations to train a robot through imitation learning.

Similar to our current work, hypernetworks [9] are utilized by some robotics CL approaches. Huang et al. [46] present an approach for continually learning robotic manipulation tasks with model-based reinforcement learning in which the dynamics model is generated by a hypernetwork [10]. In a similar vein, Schoepf et al. [47] employ a hypernetwork-generated Proximal Policy Optimization [48] agent for learning multiple manipulation tasks with model-free reinforcement learning. A hypernetwork-based solution for supervised continual-LfD is proposed in [7], where the parameters of a NODE [8] are generated with a hypernetwork that learns a sequence of real-world manipulation skills. In the present work, we also rely on hypernetworks for continual learning of robotic manipulation skills, but unlike [46], [47], our focus is on *supervised* continual learning from demonstrations, we evaluate on real-world tasks, and we assess CL performance of our robot on much longer task sequences. In contrast to [7], our approach has guarantees regarding the stability of the predicted robot trajectories. Instead of generating a single network with a hypernetwork as in [7], our hypernetworks generate two neural networks that comprise an *sNODE*. We compare our proposed models against [7] and achieve much better CL performance, especially with the size-efficient chunked hypernetworks. We also propose stochastic hypernetwork regularization with a *single* task embedding to make hypernetwork training more efficient. Additionally, the highest dimension of the trajectories used for evaluation in [7] is 3 compared to 32 in this paper. Finally, for real-world robot tasks our models predict position and orientation trajectories simultaneously (instead of using separate models [7]), and we train and evaluate our models on a much longer sequence of 9 real-world tasks compared to 4 tasks in [7].

In learning from demonstration, the dynamics model needs to learn the vector field of the demonstrated trajectories from a very limited number of demonstrations, far less than the labeled examples that are available for typical supervised learning

scenarios. Additionally, in stable-LfD, the stability guarantee imposes additional constraints that can make the learning of these vector fields even more challenging. On top of this, to learn multiple tasks we also need to mitigate the effects of catastrophic forgetting. As far as we are aware, ours is the first work that shows that continual stable-LfD is possible for real-world tasks and that the stability guarantee has a positive effect on the continual learning capability of hypernetworks.

III. BACKGROUND

The continual-LfD models and baselines in this paper are composed of two subsystems: (A) a *learning from demonstration* (LfD) system that learns motion skills from demonstration, and (B) a *continual learning* system that mitigates *catastrophic forgetting* when multiple motion skills are learned. In this section, we briefly describe the fundamentals of these subsystems.

A. Learning from Demonstration

In this paper, we focus on neural network based continual learning. Hence, we consider neural network-based approaches for learning trajectories of the robot's end-effector position and orientation from human demonstrations.

1) *Neural ODEs and Stability*: A Neural Ordinary Differential Equation solver (NODE) [8] is a neural network that learns a dynamical system directly from observations. In this approach, a fully-connected neural network $\hat{\mathbf{f}}_\theta(\mathbf{x}) : \mathbb{R}^n \rightarrow \mathbb{R}^n$ with parameters θ represents a dynamical system. By integrating this function over time, an approximate solution to the ODE system at time t can be obtained as

$$\hat{\mathbf{x}}_t = \hat{\mathbf{x}}_0 + \int_0^t \hat{\mathbf{f}}_\theta(\hat{\mathbf{x}}_\tau) d\tau \quad (1)$$

where $\hat{\mathbf{x}}_0$ is the start of the trajectory. If we have a dataset \mathcal{D} of N observed trajectories $\{\mathbf{x}_{0:T-1}^{(0)}, \dots, \mathbf{x}_{0:T-1}^{(N-1)}\}$, where each trajectory $\mathbf{x}_{0:T-1}^{(i)}$ is a sequence of T points $\mathbf{x}_t^{(i)} \in \mathbb{R}^d$. The parameters θ can be learned using the dataset \mathcal{D} by minimizing the following loss [7]:

$$\mathcal{L} = \frac{1}{2} \sum_t \|\mathbf{x}_t - \hat{\mathbf{x}}_t\|_2^2 \quad (2)$$

A basic NODE trained by minimizing Eq. (2) does not provide any formal guarantees regarding the stability of the predicted trajectories. If the learning is not successful or if the starting state of the trajectory is different from the demonstrations, then it is possible for the predicted trajectory to diverge from the goal. This can be dangerous when such a system is used to control a robot.

To solve this problem, Manek and Kolter [6] propose to jointly learn a dynamics model and a *Lyapunov* function that ensures stability. In addition to the nominal dynamics model $\hat{\mathbf{f}}_\theta(\mathbf{x}) : \mathbb{R}^n \rightarrow \mathbb{R}^n$, let $V_\gamma(\mathbf{x}) : \mathbb{R}^n \rightarrow \mathbb{R}$ (parameterized by γ) denote a Lyapunov function, which is a positive definite function, such that $V_\gamma(\mathbf{x}) \geq 0$ for $\mathbf{x} \neq 0$ and $V_\gamma(0) = 0$. The projection of $\hat{\mathbf{f}}_\theta$ that satisfies the condition

$$\nabla V_\gamma(\mathbf{x})^T \hat{\mathbf{f}}_\theta(\mathbf{x}) \leq -\alpha V_\gamma(\mathbf{x}) \quad (3)$$

ensures a stable dynamics system, where $\alpha \geq 0$ is a constant. The following function is guaranteed to produce stable trajectories [6]:

$$\begin{aligned} \mathbf{f}_\phi(\mathbf{x}) &= \text{Proj} \left(\hat{\mathbf{f}}_\theta(\mathbf{x}), \{f : \nabla V_\gamma(\mathbf{x})^T f(\mathbf{x}) \leq -\alpha V_\gamma(\mathbf{x})\} \right) \\ &= \hat{\mathbf{f}}_\theta(\mathbf{x}) - \nabla V_\gamma(\mathbf{x}) \frac{\text{ReLU}(\nabla V_\gamma(\mathbf{x})^T \hat{\mathbf{f}}_\theta(\mathbf{x})) + \alpha V_\gamma(\mathbf{x})}{\|\nabla V_\gamma(\mathbf{x})\|_2^2} \end{aligned} \quad (4)$$

where $\phi = \{\theta, \gamma\}$ represents the parameters of the nominal dynamics model and the Lyapunov function taken together. The Lyapunov function V_γ is modeled with an input-convex neural network (ICNN) [49]. During training, both the parameters of the nominal dynamics model $\hat{\mathbf{f}}_\theta(\mathbf{x})$ and the Lyapunov function V_γ are learned jointly [6] with Eq. (2). We refer to the stable dynamics model represented by Eq. (4) as *stable* NODE (*s*NODE).

2) *Learning Orientation Trajectories*: The orientation of the robot's end-effector is often encoded with unit quaternions. Since a trajectory of orientations does not lie in Euclidean space, we follow the same approach as [7], [50], [51] and project quaternions into the tangent space, which is a local Euclidean space.

Consider a trajectory of quaternions $\mathbf{q}_{0:T-1}$ comprising of a sequence of T quaternions, in which each quaternion $\mathbf{q}_t = [v_t^{(i)}, \mathbf{u}_t^{(i)}]^T$, where $\mathbf{q}_t \in \mathbb{S}^3$, $v_t \in \mathbb{R}$ and $\mathbf{u}_t \in \mathbb{R}^3$. Each quaternion $\mathbf{q}_t \in \mathbb{S}^3$ in the trajectory $\{\mathbf{q}_0, \dots, \mathbf{q}_t, \dots, \mathbf{q}_{T-1}\}$ can be projected into its corresponding rotation vector $\mathbf{r}_t \in \mathbb{R}^3$ in the tangent space using the *logarithmic map* [52] $\text{Log}(\cdot) : \mathbb{S}^3 \mapsto \mathbb{R}^3$:

$$\mathbf{r}_t = \text{Log}(\bar{\mathbf{q}}_t \otimes \mathbf{q}_{T-1}) \quad (5)$$

$$\text{where } \text{Log}(\mathbf{q}) = \begin{cases} \arccos(v) \frac{\mathbf{u}}{\|\mathbf{u}\|} & \text{if } \|\mathbf{u}\| > 0, \\ [0, 0, 0]^T & \text{otherwise.} \end{cases}$$

Here, \otimes denotes quaternion multiplication. The transformed trajectory in the tangent space can be learned with the help of Eq. (4) and Eq. (2). After the trajectories of rotation vectors have been learned, the model's predictions are also in the form of rotation vector trajectories. Each rotation vector $\hat{\mathbf{r}}_t \in \mathbb{R}^3$ in a predicted trajectory $\{\hat{\mathbf{r}}_0, \dots, \hat{\mathbf{r}}_t, \dots, \hat{\mathbf{r}}_{T-1}\}$ can be projected back to a corresponding quaternion $\hat{\mathbf{q}}_t \in \mathbb{S}^3$ on the hypersphere using the *exponential map* [52] $\text{Exp}(\cdot) : \mathbb{R}^3 \mapsto \mathbb{S}^3$:

$$\hat{\mathbf{q}}_t = \mathbf{q}_{T-1} \otimes \text{Exp}(\hat{\mathbf{r}}_t) \quad (6)$$

where

$$\text{Exp}(\mathbf{r}) = \begin{cases} \left[\cos(\|\mathbf{r}\|), \sin(\|\mathbf{r}\|) \frac{\mathbf{r}}{\|\mathbf{r}\|} \right]^T & \text{if } \|\mathbf{r}\| > 0, \\ [1, 0, 0, 0]^T & \text{otherwise.} \end{cases}$$

Similar to [7], [50], [51], we assume that the input domain of $\text{Log}(\cdot)$ is restricted to \mathbb{S}^3 except for $[1, 0, 0, 0]^T$ and the input domain of $\text{Exp}(\cdot)$ satisfies $\|\zeta\| < \pi$.

B. Continual Learning

We consider continual learning approaches from all the major families of methods in the literature [12], [34]: *dynamic architectures* (new parameters are added for each new task),

replay (past training data is stored and reused while learning a new task), and *regularization* (parameters are protected from catastrophic forgetting using regularization while learning a new task). In this section, we briefly describe the continual learning methods that are related to our proposed methods and experimental baselines.

1) *Dynamic Architectures*: A straightforward approach to continual learning is to increase the capacity of the model to learn new tasks. This can be done by learning each task with a separate network [28], or by using a dynamic architecture to only add as many parameters as needed [53], [54].

2) *Replay*: A portion of the training data (or the entire data) for each task is stored, and for every new task, the cached data from past tasks is combined with the data of the current task to train a model [7].

3) *Regularization*: Regularization-based continual learning methods append additional components to the optimization objective for learning each new task. These methods can be further divided into two groups: (i) direct regularization, and (ii) meta-model regularization.

a) *Direct Regularization*: To prevent changes to the network parameters that are *important* for solving previous tasks, a weighted L2 regularization term is added to the learning objective. Typically, the loss $\tilde{\mathcal{L}}^m$ for the m^{th} task takes the form [7]

$$\tilde{\mathcal{L}}^m = \mathcal{L}^m + c \sum_k \Omega_k^m (\theta_k^* - \theta_k)^2 \quad (7)$$

where \mathcal{L}^m is the task-specific loss (e.g. MSE loss, or cross-entropy loss, etc.), c denotes the regularization constant, and Ω_k^m is the importance of the k^{th} parameter for the m^{th} task. θ_k^* and θ_k represent the value of the k^{th} parameter before learning the current task and during the present iteration respectively. The distinguishable characteristic of these methods is that the parameters being regularized belong to the model that solves the task we are interested in (e.g. for an image classifying convolutional network, the parameters of the convolutional network are regularized directly). The different direct-regularization methods differ from each other in the way the importance term Ω_k^m is computed [31]–[33].

b) *Meta-model Regularization*: Instead of directly protecting the parameters of the model that learns the tasks under consideration, a meta-model, known as a *hypernetwork* [9], [10] is used to generate the parameters of the *task learning* model. The parameters of the hypernetwork are protected from catastrophic forgetting with regularization.

Consider that a hypernetwork with parameters \mathbf{h} generates the parameters θ^m of a task learner for the m^{th} task in a sequence of continual learning tasks. For optimizing \mathbf{h} , a two-stage process is followed [7], [10]. In the first stage, a candidate change $\Delta\mathbf{h}$ is determined such that the task-specific loss \mathcal{L}^m for the m^{th} task is minimized. The task-specific loss \mathcal{L}^m depends on the task-learner parameters θ^m (which are generated by the hypernetwork) and \mathbf{x}^m , the data for the m^{th} task. Thus,

$$\mathcal{L}^m = \mathcal{L}^m(\theta^m = \mathbf{f}(\mathbf{e}^m, \mathbf{h}), \mathbf{x}^m) \quad (8)$$

where \mathbf{f} represents the hypernetwork function and \mathbf{e}^m denotes the *task embedding vector* for the m^{th} task, that forms the input

to the hypernetwork. In the second stage, the parameters \mathbf{h} and the task embedding vector \mathbf{e}^m are optimized by minimizing the regularized loss $\tilde{\mathcal{L}}^m$ [7], [10]:

$$\begin{aligned} \tilde{\mathcal{L}}^m &= \mathcal{L}^m(\theta^m = \mathbf{f}(\mathbf{e}^m, \mathbf{h}), \mathbf{x}^m) \\ &+ \frac{\beta}{m-1} \sum_{l=0}^{m-1} \|\mathbf{f}(\mathbf{e}^l, \mathbf{h}^*) - \mathbf{f}(\mathbf{e}^l, \mathbf{h} + \Delta\mathbf{h})\|^2 \end{aligned} \quad (9)$$

Here, β denotes the regularization constant and \mathbf{h}^* denotes the hypernetwork parameters before learning the m^{th} task. For each task, a separate task embedding vector is learned and then frozen for regularizing the learning of future tasks.

Since the parameters θ^m of the task learner are produced from the final layer of the hypernetwork, the hypernetwork can be quite large. To overcome this limitation, *chunked* hypernetworks have been proposed [10], in which the parameters θ^m are produced piecemeal in segments called *chunks*. In addition to the task embedding vector \mathbf{e}^m , chunked hypernetworks make use of additional inputs called *chunk embedding vectors*. Similar to the task embedding vectors, these chunk embedding vectors are also trainable. However, a separate task embedding vector is learned for each task, whereas a single set of chunk embedding vectors is shared across all tasks and is regularized in the same way as the parameters of the hypernetwork.

IV. METHODS

The continual-LfD approach proposed in this paper consists of two sub-systems: a stable node (*sNODE*) that learns the trajectories of each task, and a hypernetwork-based continual learning mechanism that makes it possible to learn multiple tasks without revisiting data from past tasks. In this section, we present the details of our approach that results in stable trajectory predictions, improved continual learning performance, and efficient training times.

A. Time-dependent Stable NODE

We introduce an additional time input to the *sNODE* model of [6] that results in more accurate trajectory predictions. Previously, it has been shown that the addition of a time input to a NODE enables it to learn a time-dependant vector field [55], thereby improving the accuracy of the predicted trajectories [7]. Motivated by this, we extend the *sNODE* model [6] by making it time-dependant, as shown in Fig. 2. This time input needs to be provided to the nominal dynamics model $\hat{\mathbf{f}}_\theta$, as well as to the Lyapunov function V_γ . Since the resultant dynamics model for *sNODE* emerges from the combination of $\hat{\mathbf{f}}_\theta$ and V_γ , the introduction of the time input is non-trivial.

We first concatenate the time input t with the state \mathbf{x}_t to create an augmented state $\hat{\mathbf{x}}_t = [\mathbf{x}_t, t]$. The input layer of the neural network representing the nominal dynamics model $\hat{\mathbf{f}}_\theta$ is modified to accept the augmented input. We leave the output layer of $\hat{\mathbf{f}}_\theta$ unchanged and simply append 1 to the output:

$$\begin{aligned} \hat{\mathbf{f}}_\theta(\hat{\mathbf{x}}_t) &= [\dot{x}_{0_t}, \dot{x}_{1_t}, \dots, \dot{x}_{n-1_t}, \dot{t}]^T \\ &= [\dot{x}_{0_t}, \dot{x}_{1_t}, \dots, \dot{x}_{n-1_t}, 1]^T \end{aligned} \quad (10)$$

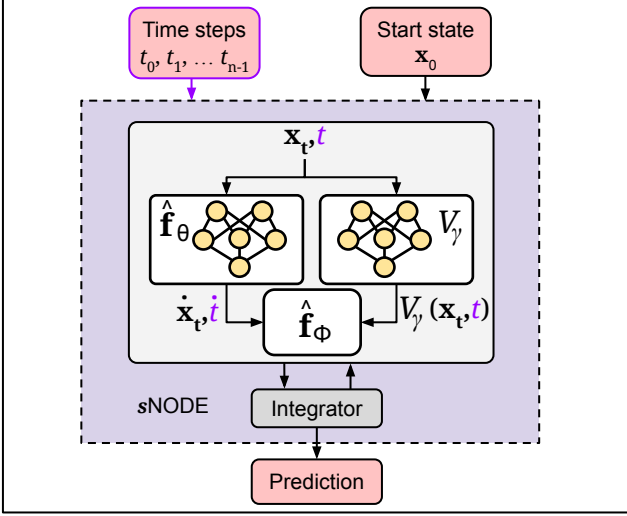


Fig. 2. Time dependent stable NODE (sNODE) architecture: time input is added to the sNODE resulting in more accurate predictions (changes are shown in purple.).

This change is done to enable the combination of $\hat{\mathbf{f}}_\theta(\hat{\mathbf{x}}_t)$ with the gradient of the Lyapunov function (in Eq. (4)), which is now defined as

$$\nabla V(\hat{\mathbf{x}}_t) = \left[\frac{\partial V}{\partial x_{0_t}}, \frac{\partial V}{\partial x_{1_t}}, \dots, \frac{\partial V}{\partial x_{n-1_t}}, \frac{\partial V}{\partial t} \right]^T \quad (11)$$

Since the Lyapunov function V_γ produces a scalar value, we only modify the input layer of the ICNN (that models the Lyapunov function) to accept an additional input and leave the output unchanged. In Fig. A.23, we show that this additional time input improves the accuracy of sNODE. We use the sNODE model with time input in all our experiments. Also, we use the NODE with time input as a comparative baseline in our experiments since the extra time input has also been shown to be beneficial for the NODE model [7].

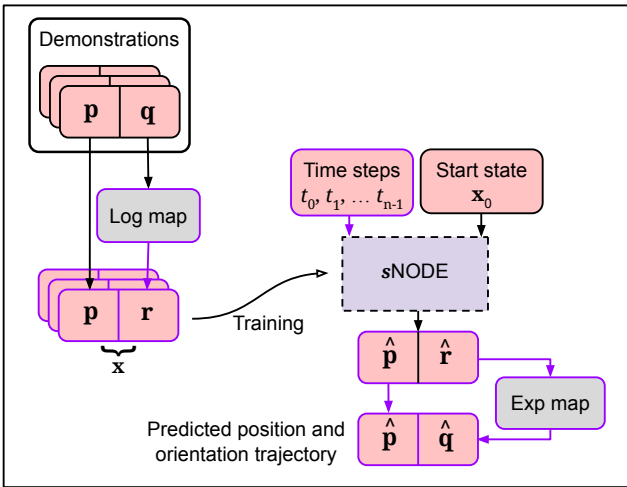


Fig. 3. Trajectories of position and orientation are learned simultaneously by projecting the orientation quaternions into rotation vectors using the Log map, learning trajectories of the positions and rotation vectors in Euclidean space, and then projecting the predicted rotation vectors back into quaternions with the help of the Exp map.

B. Learning Position and Orientation Simultaneously

For real-world LfD tasks, our models need to learn and predict trajectories of the robot's full 6-DoF pose. Previously [7], this has been achieved by using two separate NODEs (or two separate hypernetwork-generated NODEs) that are trained separately. One model learns position trajectories, and the other learns orientation trajectories. This is wasteful since the number of parameters is doubled and it takes twice as long to train.

In this paper, we propose an sNODE model that can learn position and orientation trajectories simultaneously. As shown in Fig. 3, the human demonstrations that form the training data consist of the position trajectories $\mathbf{p} = \{\mathbf{p}_0, \dots, \mathbf{p}_t, \dots, \mathbf{p}_{T-1}\}$ and orientation trajectories in the form of quaternion sequences $\mathbf{q} = \{\mathbf{q}_0, \dots, \mathbf{q}_t, \dots, \mathbf{q}_{T-1}\}$, where each $\mathbf{p}_t \in \mathbb{R}^3$ and $\mathbf{q}_t \in \mathbb{S}^3$. The orientation quaternion trajectories are converted to trajectories of rotation vectors $\mathbf{r} = \{\mathbf{r}_0, \dots, \mathbf{r}_t, \dots, \mathbf{r}_{T-1}\}$ (where each $\mathbf{r}_t \in \mathbb{R}^3$) with the help of the *logarithmic map* $\text{Log}(\cdot)$ (see Eq. (5)). The trajectories of these rotation vectors lie in the local Euclidean tangent space. The positions and rotation vectors are combined to form trajectories of 6D vectors $\mathbf{x} = \{\mathbf{x}_0, \dots, \mathbf{x}_t, \dots, \mathbf{x}_{T-1}\}$, where $\mathbf{x}_t = (\mathbf{p}_t, \mathbf{r}_t)$, which are then used to train the sNODE model using Eq. (2). For learning real-world robot tasks from human demonstrations, we found it useful to scale the rotation vectors using a constant factor before using it for training the model. After training, the sNODE predicts trajectories of 6D vectors. The orientation component is converted to the quaternion form with the *exponential map* $\text{Exp}(\cdot)$ (see Eq. (6)). Our hypernetwork-generated sNODEs also follow the same approach for real-world LfD tasks.

C. Hypernetwork Models

Hypernetworks have been demonstrated to be the best empirical choice for continual learning from demonstration in [7], where the parameters of a NODE are generated by either a chunked hypernetwork or a regular hypernetwork. In this paper, we propose chunked/regular hypernetwork models that generate the parameters of an sNODE that is comprised of two networks: (i) a nominal dynamics model that learns and predicts trajectories, and (ii) a parameterized Lyapunov function [6] that enforces stability of the predicted trajectories. This approach leads to improved continual learning performance in addition to stable trajectory predictions. In our experiments, the size of our hypernetwork \rightarrow sNODE models is kept roughly the same as the hypernetwork \rightarrow NODE models of [7].

Hypernetwork (HN): As shown in Fig. 4 (a), a regular hypernetwork generates the parameters of an sNODE $\hat{\mathbf{f}}_\phi$, as defined in Eq. (4), where $\phi = \{\theta, \gamma\}$. Here, θ represents the parameters of the nominal dynamics model $\hat{\mathbf{f}}_\theta$, and γ represents the parameters of the Lyapunov function V_γ . The parameters ϕ are generated in their entirety from the final layer of the hypernetwork. In the first step of the two-step optimization process, the candidate change $\Delta \mathbf{h}$ of hypernetwork parameters is determined by minimizing the task-specific loss given by Eq. (2):

$$\mathcal{L}^m = \mathcal{L}^m(\phi^m, \mathbf{x}^m) = \frac{1}{2} \sum_t \|\mathbf{x}_t^m - \hat{\mathbf{x}}_t^m\|_2^2 \quad (12)$$

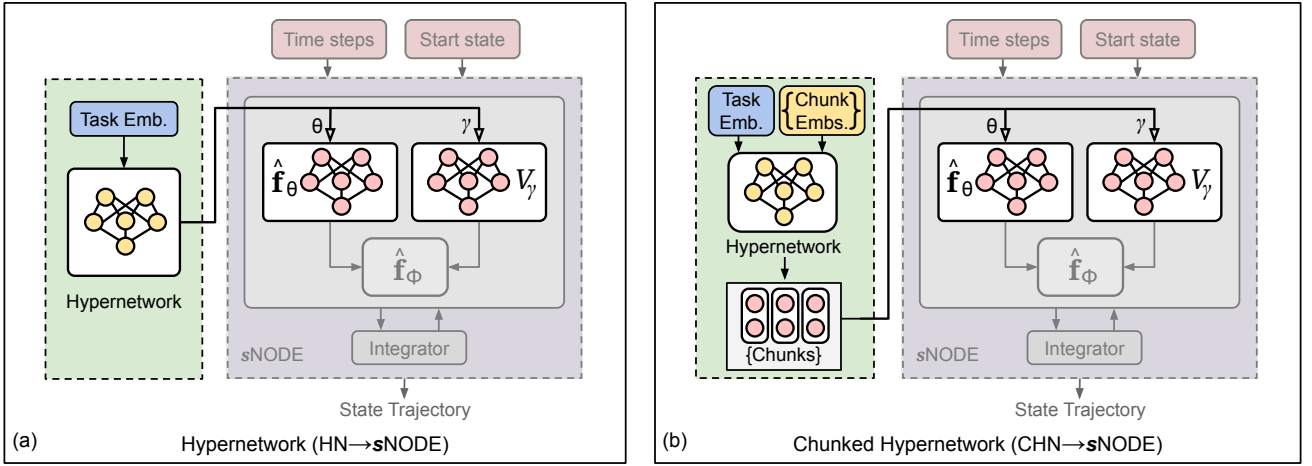


Fig. 4. (a) Architecture of the HN→sNODE model. Parameters θ and γ of the nominal dynamics model \hat{f}_θ and the Lyapunov function V_γ , respectively, of the sNODE are generated by the final layer of the Hypernetwork. (b) Architecture of the CHN→sNODE model. Parameters θ and γ of the sNODE are generated in *chunks* by the Chunked Hypernetwork, allowing for a smaller hypernetwork size. For (a) and (b), the architecture of the sNODE is the same as in Fig. 2 and is shown with muted colors here. Parameters that are learned and are task-specific are shown in blue, regularized (task-independent) learned parameters are shown in yellow, and non-trainable inputs/outputs are shown in grey. Contrary to a stand-alone sNODE, the parameters of the sNODE are not directly trainable, but are simply the outputs of the hypernetworks.

Here, $\phi^m = \{\theta^m, \gamma^m\}$ represents the sNODE parameters for the m^{th} task. $\hat{\mathbf{x}}_t^m$ and \mathbf{x}_t^m represent the prediction and ground truth at timestep t for task m respectively. The prediction $\hat{\mathbf{x}}_t^m$ is obtained with the help of Eq. (4). The entire prediction trajectory $\hat{\mathbf{x}}^m$ is obtained by integrating over the t timesteps. In the second optimization step, the hypernetwork parameters and the task embedding vector for task m are optimized as per Eq. (9). In the remainder of this paper, we refer to this model, where an sNODE is generated by a regular hypernetwork, as HN→sNODE. In our experiments, we compare against the regular hypernetwork model proposed in [7], and refer to it as HN→NODE.

Chunked Hypernetwork (CHN): As shown in Fig. 4 (b), a chunked hypernetwork generates the parameters $\phi = \{\theta, \gamma\}$ of an sNODE \hat{f}_ϕ (Eq. (4)) in segments known as *chunks*. We assemble the nominal dynamics model \hat{f}_θ and the Lyapunov function V_γ from the generated chunks. Similar to a regular hypernetwork, we use Eq. (12) and Eq. (9) as the two steps of the optimization process for training a chunked hypernetwork. We refer to this model as CHN→sNODE. We treat the CHN→NODE model from [7] as a comparative baseline, and observe significant improvements in the continual learning performance due to the introduction of sNODE.

D. Stochastic Regularization in Hypernetworks

In spite of demonstrating very good continual learning performance in a variety of domains [7], [10], [46], [56], a shortcoming of hypernetworks is that the regularization effort for training a hypernetwork increases for each new task leading to a cumulative training cost of $\mathcal{O}(N^2)$ for N tasks. This occurs due to the iteration over the stored task embeddings of all previous tasks in Eq. (9). A possible solution to this problem, as proposed in [10], is to use a random subset (of fixed size) of past task embeddings for regularization. Thus,

for learning the m^{th} task, the hypernetwork loss function in the second optimization step in Eq. (9) becomes

$$\tilde{\mathcal{L}}^m = \mathcal{L}^m(\theta^m, \mathbf{x}^m) + \frac{\beta}{|\mathcal{K}|} \sum_{\mathbf{e}^l \in \mathcal{K}}^{\mathcal{K} \sim \mathcal{U}(\mathcal{E}_{m-1})} \|\mathbf{f}(\mathbf{e}^l, \mathbf{h}^*) - \mathbf{f}(\mathbf{e}^l, \mathbf{h} + \Delta \mathbf{h})\|^2 \quad (13)$$

where \mathcal{K} denotes the random subset of task embeddings sampled uniformly from the set of all past task embeddings $\mathcal{E}_{m-1} = \{\mathbf{e}^0, \dots, \mathbf{e}^{m-1}\}$. Other symbols have the same meaning as in Eq. (9). The size of \mathcal{K} is fixed, and as long as $|\mathcal{K}| \leq m-1$ (i.e. until more tasks than the size of \mathcal{K} have been learned), \mathcal{K} simply includes all past task embeddings. Von Oswald et al. [10] show that by setting $|\mathcal{K}| = 32$, a hypernetwork is able to achieve continual learning performance which is only marginally worse than the full regularization for the *Permuted MNIST* (PMNIST) continual learning benchmark. This helps to set an upper bound on the time and effort for hypernetwork training: the cumulative training time increases quadratically till $|\mathcal{K}| \leq m-1$, after which it becomes linear.

We propose to completely remove the summation operation in Eq. (13), i.e., in each training iteration, we uniformly sample a single past task embedding from the set of all past task embeddings (i.e. $|\mathcal{K}| = 1$) and use this for regularization:

$$\tilde{\mathcal{L}}^m = \mathcal{L}^m(\theta^m, \mathbf{x}^m) + \beta \|\mathbf{f}(\mathbf{e}^k, \mathbf{h}^*) - \mathbf{f}(\mathbf{e}^k, \mathbf{h} + \Delta \mathbf{h})\|^2 \quad (14)$$

where $\mathbf{e}^k \sim \mathcal{U}(\mathcal{E}_{m-1})$

We demonstrate empirically (see Sec. VI-D), that for continual learning from demonstration of real-world LfD tasks, the performance of a hypernetwork with our proposed form of stochastic regularization is equivalent to a model where the complete regularization is used. With this proposed change, the cumulative training cost of hypernetworks for N tasks becomes $\mathcal{O}(N)$ instead of $\mathcal{O}(N^2)$ (the training time for each new task is approximately constant). This cumulative cost of $\mathcal{O}(N)$ is achieved from the very first task, unlike [10] which

requires a burn-in period with quadratic growth. We present detailed results and also discuss limitations of this form of regularization in Sec. VI-D.

V. EXPERIMENTAL SETUP

In this section, we describe our experimental setup, encompassing the computational hardware employed, the different LfD datasets we evaluate our approach on, the different metrics we report, and the baselines that we compare our approach against. Experiment hyperparameters are reported in the appendix (see Tab. A.7).

A. Hardware

All our experiments are conducted on a computing cluster comprising 16 nodes, each equipped with 125 GB of RAM, a single AMD Ryzen 2950X 16-Core processor, and 4 GeForce RTX 2070 GPUs. Each experiment runs on a single node, utilizes a restricted amount of RAM and only one GPU, making it feasible to run seamlessly on a single GPU or even on a system with only a CPU.

B. Datasets

LASA 2D: LASA [11] ($\mathcal{D}_{\text{LASA2D}}$) is a dataset of two dimensional trajectories of different shapes that is widely used in the LfD community [1], [2], [4], [7], [57] to benchmark model performance. $\mathcal{D}_{\text{LASA2D}}$ contains 30 different tasks, where each task is a collection of 7 similar demonstrations. Each demonstration in each task is a sequence of 1000 2D points. Out of the 30 tasks in $\mathcal{D}_{\text{LASA2D}}$, we use the same 26 tasks that have been used in [7] for evaluation. The other 4 tasks are omitted since they are created by merging together dissimilar trajectories. Fig. 10 shows some examples from $\mathcal{D}_{\text{LASA2D}}$. We chose this dataset since it contains a large number of diverse tasks and is particularly suitable for evaluating the continual learning capability of each model as it strives to learn all 26 tasks of the dataset one by one.

High-dimensional LASA: Although $\mathcal{D}_{\text{LASA2D}}$ provides a long sequence of tasks, all of these tasks involve only 2-dimensional trajectories. To evaluate the scalability of our approach to continual learning of high-dimensional trajectories, and since there is no existing dataset suitable for this purpose, we create high-dimensional analogues of the LASA dataset. We create three datasets $\mathcal{D}_{\text{LASA8D}}$, $\mathcal{D}_{\text{LASA16D}}$, and $\mathcal{D}_{\text{LASA32D}}$ where each dataset contains 10 tasks of 8, 16 and 32 dimensional trajectories respectively. We create these datasets by concatenating multiple tasks chosen uniformly from $\mathcal{D}_{\text{LASA2D}}$ into 1 task. For example, a single task in $\mathcal{D}_{\text{LASA32D}}$ is created by concatenating 16 tasks from $\mathcal{D}_{\text{LASA2D}}$. While concatenating the original tasks from $\mathcal{D}_{\text{LASA2D}}$ to create one task of the high-dimensional datasets, we only use unique tasks. Each high-dimensional dataset is a sequence of 10 tasks $T_{t=0:9}$, where each task contains 7 demonstrations $D_{d=0:6}$ and each demonstration is a sequence of 1000 points $P_{p=0:999}$. The dimension of these points are 8, 16, and 32 for $\mathcal{D}_{\text{LASA8D}}$, $\mathcal{D}_{\text{LASA16D}}$, and $\mathcal{D}_{\text{LASA32D}}$ respectively. An example of the tasks in $\mathcal{D}_{\text{LASA8D}}$ can be viewed in Fig. A.25.

RoboTasks9: For evaluation in the real world, we consider tasks in which both the position and orientation of the robot’s end effector vary over time. We add 5 new tasks to the 4 existing tasks of the *RoboTasks* dataset [7], creating a dataset of 9 real-world tasks which we refer to as *RoboTasks9* (\mathcal{D}_{RT9}). The 9 tasks of \mathcal{D}_{RT9} are (i) *box opening*: the lid of a box is opened, (ii) *bottle shelving*: a bottle is placed horizontally on a shelf, (iii) *plate stacking*: a plate is placed on a table, (iv) *pouring*: coffee beans are poured from a cup into a container, (v) *mat folding*: a mat is folded in half, (vi) *navigating*: an object is carried between obstacles, (vii) *pan on stove*: a pan is transferred from a hanging position to a table, (viii) *scooping*: coffee beans are scooped with a spatula, (ix) *glass-upright*: a wine glass lying on its side is made to stand upright. Tasks (v)-(ix) are created by us in this paper. Refer to Fig. 1 (d) for a visual depiction of the 9 tasks of \mathcal{D}_{RT9} . Each task of \mathcal{D}_{RT9} contains 9 demonstrations provided kinesthetically by a human. Each demonstration is a sequence of 1000 steps. In each step of each demonstration, the robot’s position $\mathbf{p} \in \mathbb{R}^3$ and orientation $\mathbf{q} \in \mathbb{S}^3$ are recorded. \mathcal{D}_{RT9} allows us to evaluate our approach on tasks that can be expected in the real-world, and the long sequence of 9 tasks is more suitable for assessing the continual learning capability of our approach compared to the much shorter sequences of real-world tasks in prior work [7], [46], [47].

C. Metrics

Trajectory Metrics: We measure the accuracy of the predicted trajectories in terms of their similarity to the ground truth demonstrations. For trajectories of the end-effector position, we report the widely-used *Dynamic Time Warping error* (DTW) [2], [7], [58]. For trajectories of the robot’s orientation, we report the commonly used *Quaternion error* [7], [50], [52].

Continual Learning Metrics: To assess the continual learning performance of our models, we report the following 6 metrics which evaluate the models according to a diverse set of criteria: (i) *Accuracy* (ACC) [59]: average accuracy of the trajectories predicted for the current and past tasks, (ii) *Remembering* (REM) [59]: a measure of how well past tasks are remembered, (iii) *Model Size Efficiency* (MS) [59]: how much the size of the model grows compared to its initial size, (iv) *Sample Storage Size Efficiency* (SSS) [59]: how the data storage requirements of a model grows when training data of past tasks is stored, (v) *Time Efficiency* (TE) [7]: increase in training duration with the number of tasks relative to the time taken to learn the first task, and (vi) *Final Model Size* (FS) [7]: A measure of the final parameter size of a model relative to the other models it is compared against. Each of these metrics lies in the range 0 (worst) to 1 (best). Using the set of individual continual learning metrics $\mathcal{C} = \{\text{ACC}, \text{REM}, \text{MS}, \text{SSS}, \text{TE}, \text{FS}\}$, we also report the overall continual learning metrics $\text{CL}_{\text{score}} = \sum_i^{n(\mathcal{C})} c_i$ and $\text{CL}_{\text{stability}} = 1 - \sum_i^{n(\mathcal{C})} \text{STDEV}(c_i)$ [59].

Stability Metrics: We assess the stability (convergence) of the trajectories predicted by our models in two ways. Firstly, we initialize a model at a starting position that is different from the demonstration and then measure the distance between the final

point of the predicted trajectory and the goal (final point of the demonstration). For stable trajectories, this Δ *goal-position* will be small. Secondly, we assess whether the trajectories predicted by the model move away from the goal. For this, we make the models predict trajectories of steps greater than those seen in the demonstrations (e.g. demonstrations are of 1000 steps, the model makes predictions for 1100 or 1200 steps). The ideal model's predicted trajectory in this case should terminate close to the goal irrespective of the number of extra steps.

D. Baselines

Our comparative baselines include CL methods from all families. For each CL method, we consider two versions: one where the task learner is a NODE and another where the task learner is a *s*NODE. We compare our proposed hypernetwork models (HN \rightarrow *s*NODE, CHN \rightarrow *s*NODE) against HN \rightarrow NODE, CHN \rightarrow NODE [7] and the below baselines:

Single model per task (SG): A single NODE/*s*NODE is used to learn a single task, and is frozen after the task is learned. For predicting the trajectories of the m^{th} task, the m^{th} model is chosen. This setting acts as an upper performance baseline, as the learning of new tasks does not induce forgetting in the previous models.

Finetuning (FT): A single NODE/*s*NODE is trained on the first task, and then finetuned to learn each subsequent task. This setting acts as the lower performance baseline, since finetuning overwrites the knowledge of past tasks.

Replay (REP): The data of each task is stored and replayed for the training of a NODE/*s*NODE model on each subsequent task. Following [7], we keep the number of training iterations constant for each task.

Synaptic Intelligence (SI): This setting is similar to FT, but for learning a new task, a regularization loss (Eq. (7)) is

used to protect the parameters that are deemed important for remembering past tasks. Refer to [7], [32] for details.

Memory Aware Synapses (MAS): Similar to SI, this is also a direct regularization baseline that uses Eq. (7). The difference is only in the computation of parameter importance. Refer to [7], [33] for further details.

Since during inference we need to tell the model which task it should predict trajectories for, the models of FT, REP, SI, and MAS are task-conditioned [7] by an additional input in the form of a task embedding vector.

VI. RESULTS

We present the results of our experiments on the datasets described in Sec. V-B. Experiment hyperparameters (Tab. A.7) and additional results can be found in the appendix.

A. Long Sequence of Tasks: LASA 2D

We consider all the 7 different types of continual learning methods (SG, FT, REP, SI, MAS, HN, CHN) as described in Sec. V, and for each of these CL methods, we consider 2 kinds of task learning approaches: NODE and *s*NODE. Thus, in total we have 14 different models, each of which we continually train on the 26 tasks of $\mathcal{D}_{\text{LASA2D}}$. After a model has finished learning a task, we evaluate the trajectory errors of the predictions made by the model for the current task as well as all previous tasks. This is repeated for each task, e.g. after learning the m^{th} task in a sequence of T tasks, a model is evaluated on tasks $(0, 1, \dots, m)$. This is repeated for all tasks, i.e for $m = 0, 1, \dots, T - 1$. Each experiment is repeated for 5 independent seeds.

We record all the predicted trajectory errors and report the overall errors in Fig. 5 that shows that amongst all the methods, FT, SI, and MAS produce high errors (for both NODE and *s*NODE), and the hypernetwork methods (HN, CHN) perform on par with the upper baselines SG and REP. The comparison between NODE and *s*NODE for SG shows that there is no difference in the performance. However, for all the other CL methods that produce low errors (REP, HN, CHN), the errors for *s*NODE are lower than those for NODE. This difference is most prominent for CHN (the model with the smallest size) where CHN \rightarrow *s*NODE performs a lot better than CHN \rightarrow NODE.

Fig. 6 shows a more detailed view of the prediction errors after each task is learned during the training process for the CL methods that work the best (SG, REP, HN, and CHN). Here, it can be seen that the CHN \rightarrow *s*NODE model clearly outperforms the CHN \rightarrow NODE model. With *s*NODE, the chunked hypernetwork is able to learn and remember all 26 tasks of the dataset and its performance is comparable to that of the much larger HN and also to the upper baseline SG. On the other hand, a CHN \rightarrow NODE model can only remember a few tasks and starts to exhibit high errors after task 9. Marginal improvements in performance can also be observed for REP and HN when *s*NODE is used.

Fig. 7 shows that CHN models for both NODE and *s*NODE are the smallest among all the compared models. In spite of having the least number of parameters, the performance of CHN \rightarrow *s*NODE is comparable to that of HN and the upper

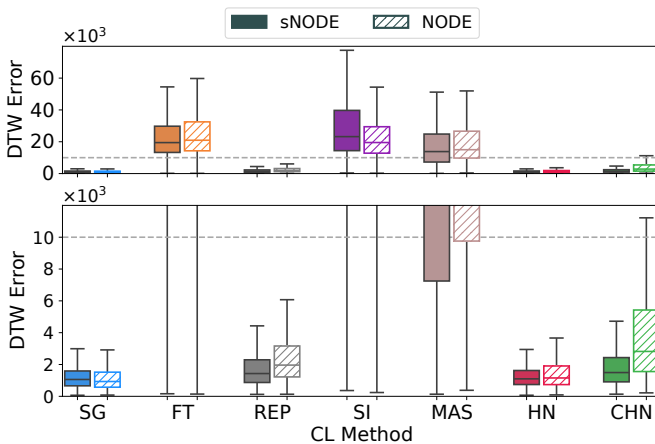


Fig. 5. DTW errors (lower is better) of all predictions while learning the LASA 2D tasks. The bottom row shows a zoomed-in view of the top plot, and the dashed gray line is a reference for comparing the scales of the two plots. Solid boxes depict *s*NODE and hatched boxes depict NODE. With *s*NODE as the task learner, HN \blacksquare and CHN \blacksquare outperform regularization based methods (SI \blacksquare , MAS \blacksquare), and perform on par with the upper baselines SG \blacksquare and REP \blacksquare . For SG, there is no perceivable difference between NODE \hatchedbox and *s*NODE \blacksquare , but *s*NODE improves the continual learning performance of REP (\blacksquare vs \hatchedbox), HN (\blacksquare vs \hatchedbox) and most considerably that of the smallest model CHN (\blacksquare vs \hatchedbox). Results shown are obtained with 5 independent seeds.

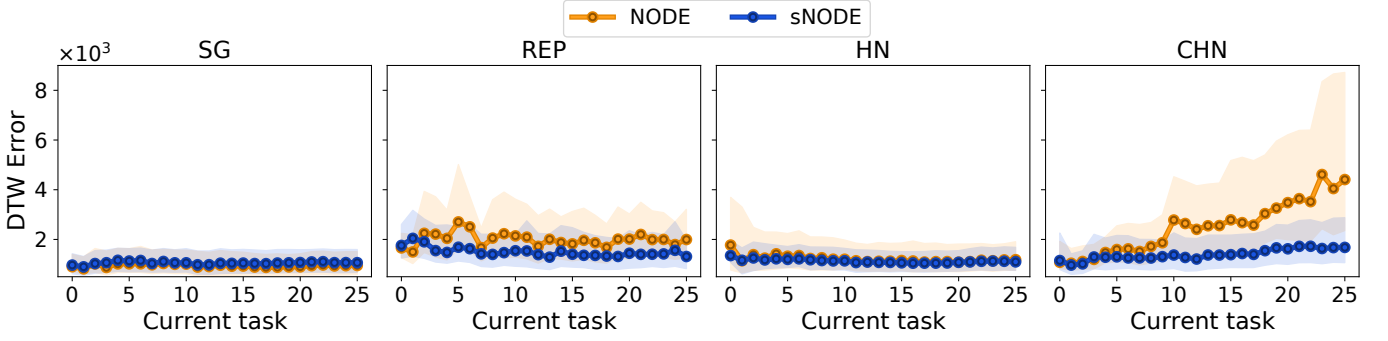


Fig. 6. s NODE \bullet improves continual learning performance compared to NODE \bullet : DTW errors (lower is better) of trajectories predicted by SG, REP, HN, and CHN while learning the tasks of the LASA dataset are shown. The x-axis shows the current task. After learning each new task, the current and all previous tasks are evaluated. The DTW errors of these predictions are shown on the y-axis. Points show the medians and the shaded region represents the inter-quartile range of results for 5 independent seeds. The performance of SG with NODE and s NODE is equivalent and there are minor improvements for REP and HN with an s NODE. CHN $\rightarrow s$ NODE is able to learn and remember all 26 tasks, while CHN \rightarrow NODE starts producing high errors after task 9.

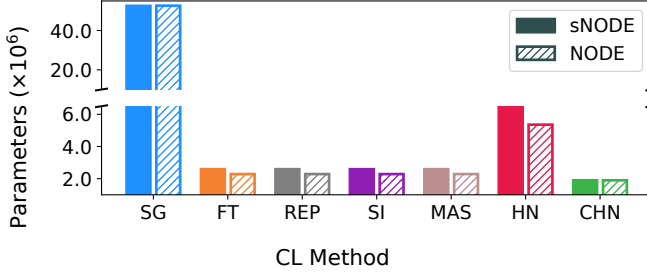


Fig. 7. Parameter counts after learning all 26 tasks of the LASA 2D dataset. We do not show the storage needed by REP to store the data of all tasks. Despite having much fewer parameters than SG (which uses 26 networks to learn 26 tasks) and HN, the performance of CHN $\rightarrow s$ NODE is equivalent to these larger models.

baseline SG, both of which have many more parameters. The network architectures of all the models are reported in Tab. A.7 in the appendix.

Next, we report the continual learning metrics that measure the different trade-offs made by the models for learning all the tasks of the LASA dataset. For measuring the continual learning metrics, each prediction has to be classified as either accurate or inaccurate by setting a threshold on the DTW error. For this, we use the same threshold value of 2191 used in [7]. The resulting continual learning metrics for the methods that perform well are reported in Figs. 8 and 9 (see Tab. A.1 for the complete set of CL metrics for all methods).

Fig. 8 shows that amongst the s NODE models that perform well, HN and CHN perform consistently well across all continual learning metrics, unlike SG and REP. Fig. 9 shows that CHN $\rightarrow s$ NODE outperforms CHN \rightarrow NODE in multiple CL metrics. s NODE also improves the performance of HN. In fact, HN $\rightarrow s$ NODE and CHN $\rightarrow s$ NODE achieve the best overall continual learning score amongst all the 14 models (see Tab. A.1 for details). Fig. 10 shows qualitative results for CHN \rightarrow NODE and CHN $\rightarrow s$ NODE for $\mathcal{D}_{\text{LASA2D}}$. It can be seen that CHN $\rightarrow s$ NODE predicts much more accurate trajectories. We also conduct stability tests to demonstrate

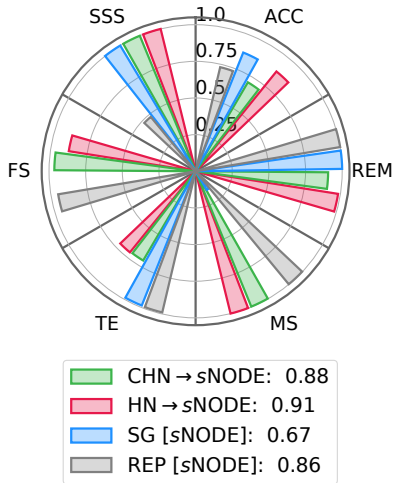


Fig. 8. Continual learning metrics (0:worst-1:best) for SG, REP, HN, and CHN with s NODE as the task learner for the LASA 2D dataset. Overall CL score is shown in the legend. SG performs poorly in terms of MS and FS, and REP has a low score in SSS. HN and CHN are the *only* models that perform consistently across all continual learning metrics, and HN $\rightarrow s$ NODE achieves the best overall CL score.

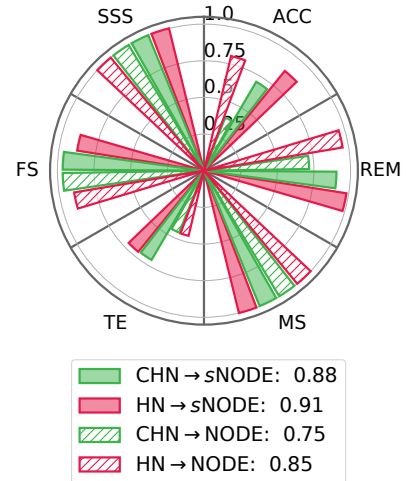


Fig. 9. Continual learning metrics (0:worst-1:best) for CHN \rightarrow NODE, HN \rightarrow NODE, CHN $\rightarrow s$ NODE and HN $\rightarrow s$ NODE for the LASA 2D dataset. Overall CL score is shown in the legend. CHN $\rightarrow s$ NODE outperforms CHN \rightarrow NODE for multiple CL metrics such as ACC, REM and TE.

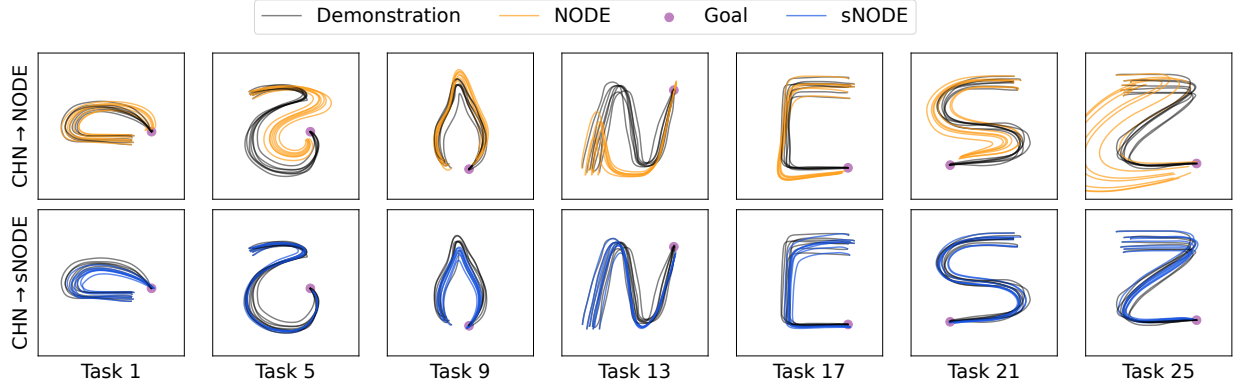


Fig. 10. Qualitative examples of predictions made for the LASA 2D dataset. CHN→NODE produces wrong predictions for many tasks, but CHN→sNODE does not. Both models learn a time-dependant vector field. As it is not feasible to plot such a 3D vector field in a 2D plot, we do not show it here.

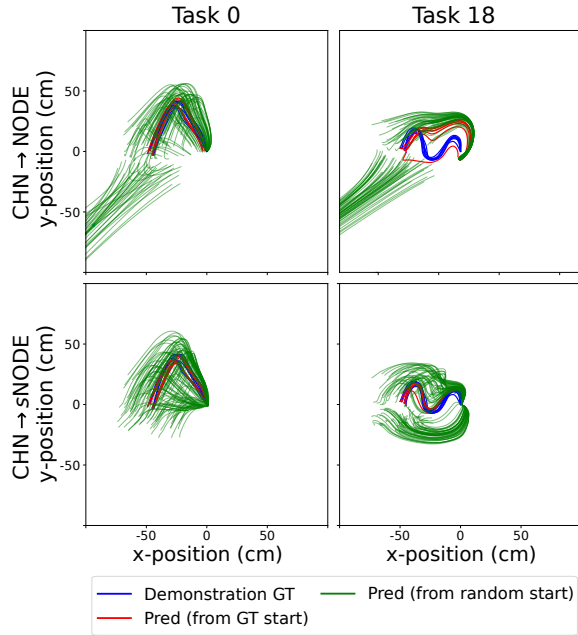


Fig. 11. Qualitative examples of predictions produced by CHN→NODE, and CHN→sNODE for 2 tasks from $\mathcal{D}_{\text{LASA2D}}$, where 100 different starting positions are chosen randomly from within a circle of radius 25 cm around the ground truth starting position. The predictions of CHN→sNODE converge near the goal, while CHN→NODE exhibits severe divergence. Both models learn a time-dependant vector field. As it is not feasible to plot such a 3D vector field in a 2D plot, we do not show it here.

the robustness of our models to novel starting positions not contained in the demonstrations. Fig. 11 shows qualitative examples in which CHN→sNODE converges near the goal but CHN→NODE exhibits divergence after starting from the same set of novel initial positions (refer to Sec. F in the appendix for further details and quantitative results of our experiments on stability).

B. High-dimensional Trajectories: LASA 8D, 16D, 32D

The high-dimensional LASA datasets ($\mathcal{D}_{\text{LASA8D}}$, $\mathcal{D}_{\text{LASA16D}}$, $\mathcal{D}_{\text{LASA32D}}$) represent a more difficult learning challenge that is designed to further test the continual learning capabilities and scalability of our models. For each of these high-dimensional datasets, we repeat the same experiments as for $\mathcal{D}_{\text{LASA2D}}$.

We evaluate the CL methods SG, FT, REP, HN, and CHN, and consider two versions of each CL method, corresponding to NODE and sNODE. We omit the direct regularization-based methods SI and MAS due to their poor performance on $\mathcal{D}_{\text{LASA2D}}$, but include FT as a lower performance baseline for reference. All experiments are repeated 5 times with independent seeds.

Fig. 12 shows the overall errors for the current and past tasks for all 10 tasks during training for the methods that perform well. The median DTW values for FT for the different datasets

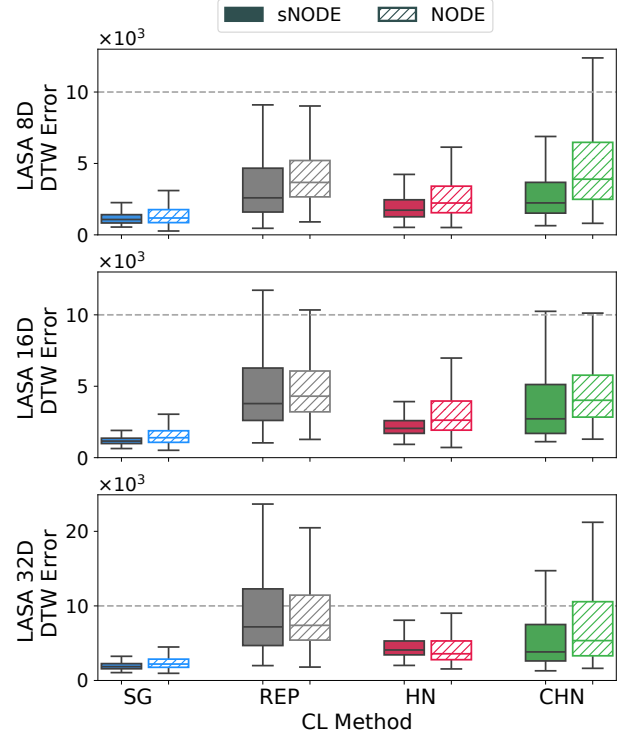


Fig. 12. Comparison of the DTW errors (lower is better) of all predictions while learning the tasks of the high-dimensional LASA datasets. Solid boxes depict sNODE and hatched boxes depict NODE. The dotted gray line is a reference for comparing the scales of the plots. For SG, there is little difference between NODE and sNODE, but sNODE improves the continual learning performance of CHN→sNODE over CHN→NODE, most prominently for LASA 8D and LASA 32D. Results shown are obtained with 5 independent seeds.

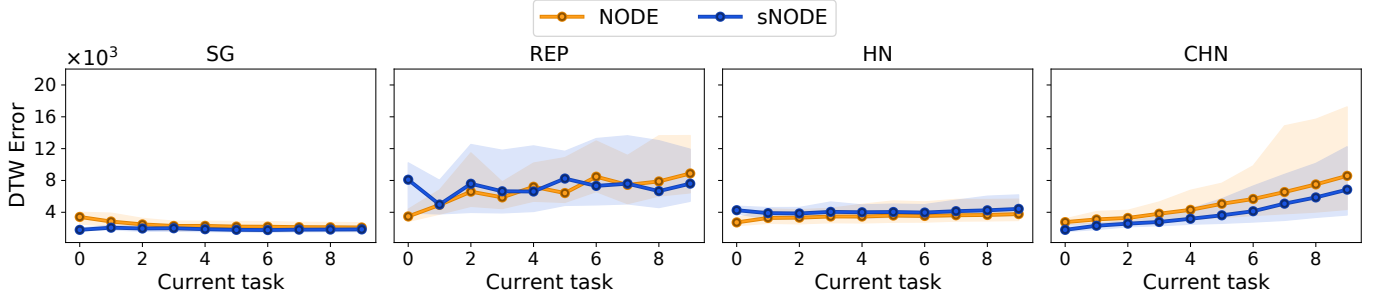


Fig. 13. DTW errors of trajectories predicted by SG, REP, HN, and CHN while learning the tasks of the LASA 32D dataset (lower is better). The x-axis shows the current task. After learning each new task, the current and all previous tasks are evaluated. The DTW errors of these predictions are shown on the y-axis. Lines show the medians and the shaded region represents the inter-quartile range of results for 5 independent seeds. The performances of SG and HN with NODE and s NODE are equivalent. CHN $\rightarrow s$ NODE produces lower median errors than CHN \rightarrow NODE and with lower variability in the results.

range from 56×10^3 to 151×10^3 and are not shown in this plot due to the much higher scale of these errors. It can be seen that the performance of HN $\rightarrow s$ NODE is close to that of the upper baseline SG. CHN $\rightarrow s$ NODE performs better than REP (both NODE and s NODE) as well as CHN \rightarrow NODE.

The evaluation errors of the predictions made for the current and past tasks after learning each individual task of $\mathcal{D}_{\text{LASA}32\text{D}}$ during training are shown in Fig. 13 (see Fig. A.24 in the appendix for the results of all the high-dimensional LASA datasets). Here, we only show the best performing methods, and omit FT due to the much higher scale of its errors. In Fig. 13, it can be seen that CHN $\rightarrow s$ NODE produces lower errors with less variability compared to CHN \rightarrow NODE. This highlights the positive influence that stability has towards improving the performance of CHN. For both the upper baseline SG and HN, the difference between NODE and s NODE is negligible. The REP baseline performs relatively poorly (for both NODE and s NODE).

Although CHN $\rightarrow s$ NODE produces higher errors than SG, note that CHN $\rightarrow s$ NODE uses only a single model (unlike SG) and does not revisit data of past tasks (unlike REP). For each dataset, the size of CHN $\rightarrow s$ NODE is much smaller than the overall size of the corresponding SG model (around 6-7 times smaller). This is also reflected in the continual learning metrics of the models for the high-dimensional LASA datasets (see complete set of CL metrics in Tabs. A.2, A.3 and A.4 for $\mathcal{D}_{\text{LASA}8\text{D}}$, $\mathcal{D}_{\text{LASA}16\text{D}}$, and $\mathcal{D}_{\text{LASA}32\text{D}}$ respectively). The hypernetwork models using s NODE (HN $\rightarrow s$ NODE,

CHN $\rightarrow s$ NODE) exhibit the best overall continual learning performance across all the high-dimensional LASA datasets.

With an increase in the trajectory dimension, the difficulty of the continual learning process also increases. To analyze the performance of the CHN models as the trajectory dimension increases, we plot the overall errors for the CHN and SG models for all the LASA datasets (including $\mathcal{D}_{\text{LASA}2\text{D}}$) side by side in Fig. 14. Here, it can be seen that for both NODE and s NODE, the errors produced by CHN increase as the trajectory dimension increases from 2 to 32. However, the performance degradation is much more severe for NODE than for s NODE.

C. Real-world Tasks: RoboTasks9

In this section, we evaluate our approach on the 9 real-world tasks of $\mathcal{D}_{\text{RT}9}$. In each task, trajectories of both the position and orientation of the end-effector of the robot need to be predicted. We evaluate and compare SG, FT, REP, HN and CHN on $\mathcal{D}_{\text{RT}9}$. In these experiments, 2 versions of each baseline are tested: one where the task learner is a NODE [7], and another where the task learner is an s NODE. As proposed in Sec. IV-B, our models predict positions and orientations simultaneously.

We train the 10 different models continually on the 9 tasks of $\mathcal{D}_{\text{RT}9}$. After each task (in the sequence of 9 tasks) is learned, we evaluate each model on the task it has just learned, as well as on all the previous tasks. All experiments are repeated 5 times with independent seeds. In Fig. 15, we compare the overall evaluation errors produced by these models while learning the tasks of $\mathcal{D}_{\text{RT}9}$. FT is excluded due to its high errors (median DTW errors for FT lie between 29×10^3 and 35×10^3 , and median Quaternion errors lie between 0.26 and 0.33 radians). It can be seen in Fig. 15 that the position (DTW) and orientation (Quaternion) errors produced by CHN $\rightarrow s$ NODE and HN $\rightarrow s$ NODE are close to those of the upper baseline SG- s NODE (which uses a different model for each task) and REP- s NODE (which reuses the training data from all the past tasks). It can also be observed that s NODE improves the performance of REP, HN and CHN in both trajectory metrics (DTW and Quat. error), while SG with s NODE performs almost identically to SG with NODE with some minor improvement in Quaternion error. Overall, the performance of CHN improves the most when stability is introduced with s NODE.

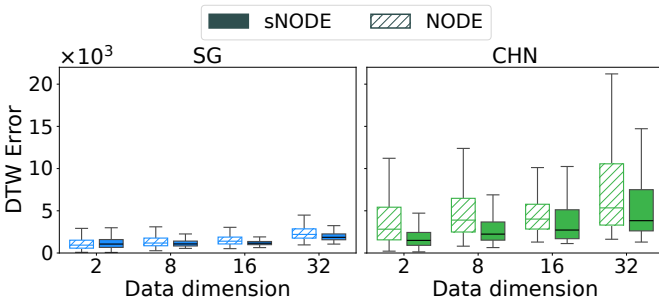


Fig. 14. Comparison of the DTW errors (lower is better) for different dimensions of the trajectories of all the LASA datasets. With an increase in dimensionality, learning becomes more difficult, but CHN $\rightarrow s$ NODE degrades less than CHN \rightarrow NODE.

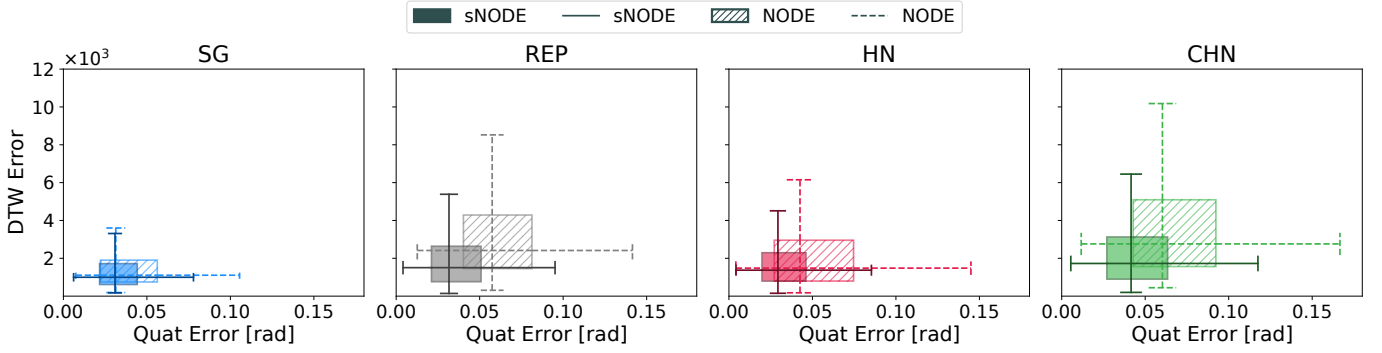


Fig. 15. 2D boxplots showing the position errors (DTW) in the y-axis, and orientation errors (quaternion error) in the x-axis of all predictions while learning the tasks of the RoboTasks9 dataset. Solid boxes depict s NODE and hatched boxes depict NODE. CHN $\rightarrow s$ NODE and HN $\rightarrow s$ NODE are among the best performing methods in spite of using a single model (unlike SG) and not retraining on past demonstrations (unlike REP). SG has almost the same performance for s NODE and NODE (only minor improvement in quat error). All other methods improve when s NODE is used. CHN $\rightarrow s$ NODE shows the biggest improvement over CHN \rightarrow NODE.

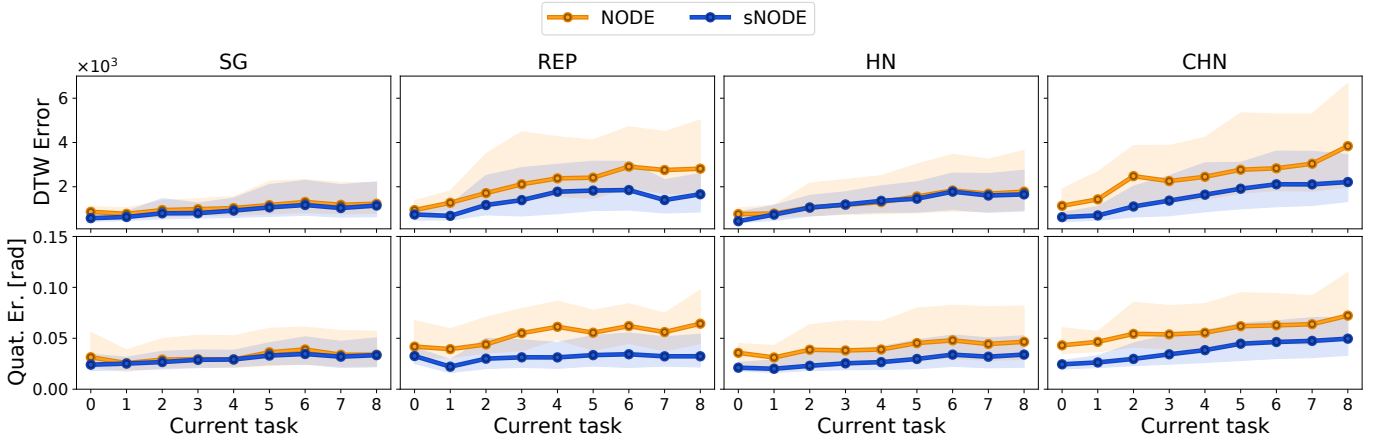


Fig. 16. Position (top) and orientation (bottom) errors of SG, REP, HN, and CHN for the RoboTasks9 dataset (lower is better). The x-axis shows the current task, and the y-axis shows the evaluation errors for the current and all previous tasks. Lines and shaded regions show the medians and inter-quartile ranges respectively for 5 independent seeds. SG with NODE and s NODE is equivalent, but there are improvements for REP, HN and CHN with s NODE. CHN $\rightarrow s$ NODE produces lower median errors than CHN \rightarrow NODE and with much less variability in the results.

While Fig. 15 shows the overall prediction errors for each method, in Fig. 16, we show a more granular view of this result to illustrate how the prediction error changes during the sequential training as more tasks are learned. The plots in the top row of Fig. 16 show the position errors, and the bottom row shows the orientation errors for SG, REP, HN, and CHN. These results also confirm that s NODE greatly improves the performance of the continual learning models, particularly REP and CHN.

Next, we evaluate the continual learning performance of the different methods on \mathcal{D}_{RT9} . We empirically set a threshold of 3000 on the DTW position error and a threshold of 0.08 radians (≈ 5 degrees) on the orientation error. These thresholds are stricter than the ones used in [7] (where the DTW threshold was 7191 and the orientation error threshold was 10 degrees), and allow us to set a higher bar for evaluating the continual learning performance of the models under consideration. The continual learning metrics for the position predictions of SG, REP, HN and CHN are reported in Figs. 17 and 18 (see Tab. A.5 and Tab. A.6 for the complete table of CL metrics for both position and orientation for all methods). Fig. 17 shows that among the s NODE models, CHN $\rightarrow s$ NODE is the only method with

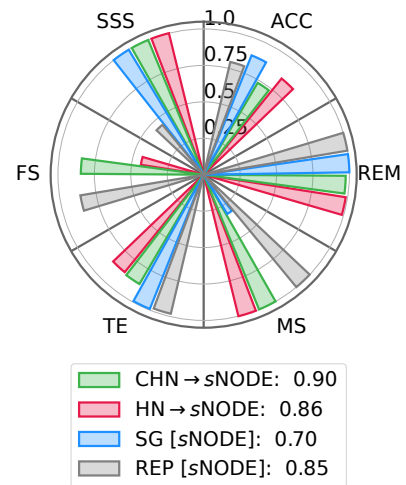


Fig. 17. Continual learning metrics (0:worst-1:best) for SG, REP, HN, and CHN with s NODE as the task learner for the RoboTasks9 dataset. Overall CL scores are shown in the legend. CHN is the only method that performs consistently across all continual learning metrics and has the highest CL score.

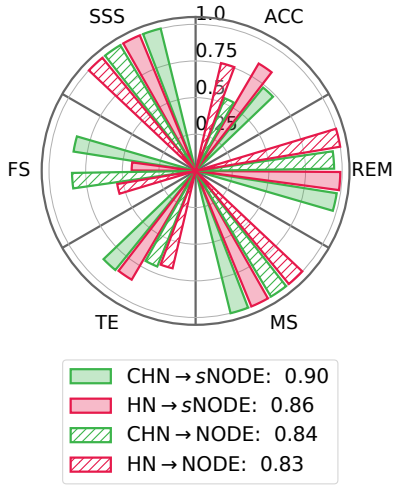


Fig. 18. Comparison of continual learning metrics (0:worst-1:best) for HN, and CHN with *s*NODE and NODE as the task learner for the RoboTasks9 dataset. Overall CL scores are shown in the legend. CHN→*s*NODE is the only method that performs consistently across all continual learning metrics and has the highest CL score.

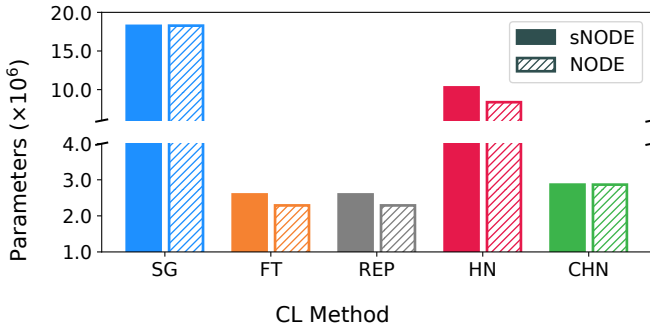


Fig. 19. Parameter counts after learning all 9 tasks of the RoboTasks9 dataset. Even with much fewer parameters than SG and HN, the performance of CHN→*s*NODE is equivalent to these larger models.

good scores for all CL metrics and thus achieves the highest overall CL score. In Fig. 18, it can be seen that the *s*NODE models of both HN and CHN outperform the NODE models, with CHN→*s*NODE exhibiting very good performance in key metrics such as ACC (*accuracy*), REM (*remembering*), and FS (*final model size*) that results in the best overall CL score among all methods.

Overall, CHN→*s*NODE offers the best trade-off for continual learning among the methods we evaluate: its size is relatively small compared to SG and HN (the model sizes are shown in Fig. 19), it can learn and remember multiple tasks without forgetting, it does not need to store and retrain on demonstrations of past tasks (unlike REP), and it predicts stable trajectories which also helps in improving its performance over CHN→NODE. Fig. 22 shows qualitative examples of the predictions for \mathcal{D}_{RT9} , where it can be seen that CHN→*s*NODE produces much lower errors than CHN→NODE. Videos of the robot performing the tasks of \mathcal{D}_{RT9} can be viewed at <https://youtu.be/xDgTvWADoyA>.

D. Stochastic Hypernetwork Regularization

A limitation of using hypernetworks for continual learning [7], [10] is that the cumulative training time of a hypernetwork increases quadratically with the number of tasks [7], [10]. To overcome this limitation, only a single randomly sampled past task embedding can be used for regularization (as proposed in Sec. IV-D). This leads to a cumulative training time cost of $\mathcal{O}(N)$ for N tasks (each new task is learned in roughly the same amount of time) instead of $\mathcal{O}(N^2)$ for the fully-regularized hypernetwork (using all past task embeddings for regularization). To show this experimentally, we train three different types of CHN→*s*NODE models on the RoboTasks9 dataset, differentiated by the way regularization is performed:

- (i) *Full regularization*: A CHN→*s*NODE model is trained using full hypernetwork regularization [10] in which the task embeddings of all past tasks are used for regularization while learning the current task (as per Eq. (9)). This is the same as the CHN models used in all the previous experiments. We refer to this model as *CHN-all*.
- (ii) *Set-based regularization*: Here, the task embeddings of a fixed number of randomly selected past tasks are considered for regularization [10] (as per Eq. (13)). We consider 2 versions of this model: *CHN-3* and *CHN-5*, which use 3 and 5 randomly selected past task embeddings for regularization respectively.

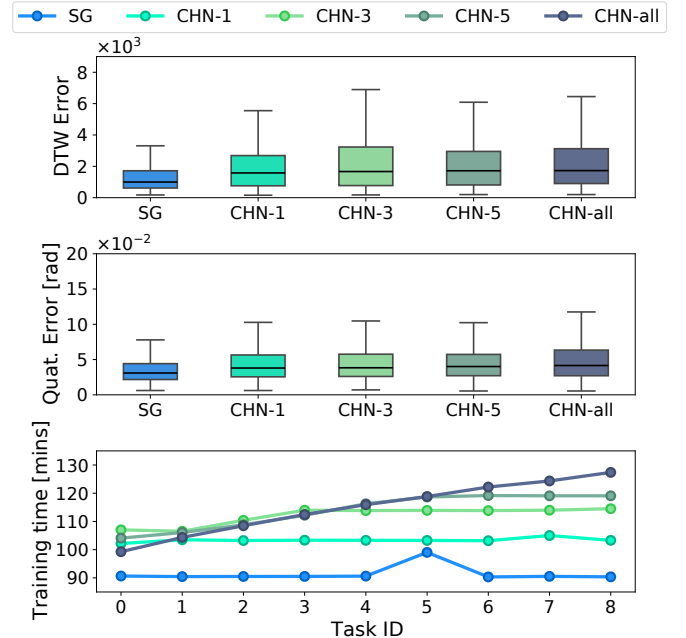


Fig. 20. Stochastic regularization in CHN→*s*NODE for the RoboTasks9 dataset: (top) position errors, (middle) orientation errors, and (bottom) training time for each task. The upper baseline SG (using *s*NODE) provides the reference for good performance, but has many more parameters than the CHN models. CHN-1 (ours), CHN-3, and CHN-5 use 1, 3 and 5 randomly selected task embeddings for regularization respectively. CHN-all uses all available task embeddings. CHN-1 performs equivalently to the other models, but its training time for each new task stays roughly the same, leading to cumulative training cost of $\mathcal{O}(N)$ for N tasks. The cumulative cost for CHN-3, and CHN-5 increases quadratically till 3 and 5 tasks are learned respectively. CHN-all has a cumulative cost of $\mathcal{O}(N^2)$ for N tasks.

(iii) *Single task embedding regularization*: In each iteration during training, a single task embedding is uniformly sampled from the list of all past task embeddings and is used for regularization (as per Eq. (14) proposed by us in Sec. IV-D). We refer to this model as *CHN-1*.

We train all 4 models (CHN-all, CHN-5, CHN-3, and CHN-1) on the 9 tasks of \mathcal{D}_{RT9} , and repeat the experiment 5 times with independent seeds. We use the same hyperparameters (details in Tab. A.7) that were used for the results reported in Sec. VI-C. Similar to before, after each task is learned, we evaluate each model on the current task as well as all the past tasks and repeat this process for all tasks in the sequence. Fig. 20 (top and middle) shows the errors of the trajectory predictions (positions and orientations) during these evaluations. For reference, we also show the performance of the upper baseline SG in the same plot. In Fig. 20 (bottom), we show the time required for learning each task in the 9-task sequence of \mathcal{D}_{RT9} . In Fig. 20 (top and middle), the performance of CHN-1 is equivalent to the other CHN models as well as to the upper baseline SG, i.e. performance of CHN is not impacted by the number of task embeddings used for regularization. However, the use of a single task embedding for regularization enables CHN-1 to achieve $\mathcal{O}(N)$ growth in the cumulative training time for N tasks compared to the $\mathcal{O}(N^2)$ growth for CHN-all, as shown in Fig. 20 (bottom). CHN-3 and CHN-5 also have $\mathcal{O}(N^2)$ growth till 3 and 5 tasks respectively are learned. The performance of SG is marginally better than that for CHN-1, but note that SG uses a separate model for each task resulting in a much larger overall parameter size (as shown in Fig. 19) and much worse overall continual learning performance (as shown in Fig. 17).

We also train the CHN \rightarrow sNODE model for CHN-1 on all the LASA datasets (containing 2, 8, 16 and 32-dimensional trajectories) using the same hyperparameters that are used in the experiments in Sections VI-A and VI-B. The results are presented in Fig. 21, where CHN-1 is compared against CHN-all and SG (both with sNODE). For all LASA datasets, the median errors of CHN-1 are comparable to that of the fully regularized CHN-all model. However, the variability in the

results for CHN-1 is much larger than CHN-all for $\mathcal{D}_{\text{LASA2D}}$, $\mathcal{D}_{\text{LASA16D}}$, and $\mathcal{D}_{\text{LASA32D}}$. For $\mathcal{D}_{\text{LASA8D}}$, the performance of CHN-1 is equivalent to that of CHN-all (similar to the results for \mathcal{D}_{RT9}).

From the results in Fig. 20 and Fig. 21, it can be seen that CHN-1 performs as well as CHN-all (in terms of prediction errors) for the real-world LfD tasks of \mathcal{D}_{RT9} (9 tasks, each containing 6-dimensional trajectories) and $\mathcal{D}_{\text{LASA8D}}$ (10 tasks, each containing 8-dimensional trajectories). CHN-1 exhibits reduced performance compared to CHN-all when the number of tasks is high ($\mathcal{D}_{\text{LASA2D}}$), or when each task involves high-dimensional trajectories ($\mathcal{D}_{\text{LASA16D}}$, $\mathcal{D}_{\text{LASA32D}}$).

The regularization strength (i.e. how well the hypernetwork tries to remember past tasks) for CHN-1 is dependent on the number of times each past task embedding is sampled during training. Thus if the number of tasks is high (as in $\mathcal{D}_{\text{LASA2D}}$), it is possible that each task embedding is not sampled frequently enough to ascertain that all past tasks are remembered equally well. Also, if the number of training iterations per task is low compared to the task complexity (in terms of trajectory dimensions), stochastic regularization with a single task embedding can also suffer due to insufficient regularization. For $\mathcal{D}_{\text{LASA2D}}$, we use 1.5×10^4 iterations/task (based on [7]), and for \mathcal{D}_{RT9} (4×10^4 iterations/task) and $\mathcal{D}_{\text{LASA8D}}$ (6×10^4 iterations/task), we scale the iterations approximately linearly based on the trajectory dimensions. However, for the higher-dimensional $\mathcal{D}_{\text{LASA16D}}$ (7×10^4 iterations/task) and $\mathcal{D}_{\text{LASA32D}}$ (8×10^4 iterations/task) datasets, we used much fewer iterations than that suggested by the dimension-based proportional scaling as we wanted to limit the overall run time of our large number of experiments.

To make CHN-1 more effective, a naive solution can be to simply increase the number of training iterations per task. A better approach can be to use a priority-based sampling of past task embeddings during regularization such that important task embeddings are sampled more frequently.

The stochastic regularization process of CHN-1 proposed in this paper is an effective strategy for continually learning real-world LfD tasks (\mathcal{D}_{RT9}) or tasks of a similar nature ($\mathcal{D}_{\text{LASA8D}}$). For these situations, the cumulative training cost is reduced to $\mathcal{O}(N)$ from $\mathcal{O}(N^2)$ without any loss in performance. In the future, we will investigate approaches to make CHN-1 an effective strategy for more complex scenarios involving higher number of tasks and/or high-dimensional trajectories.

VII. DISCUSSION

Robots trained with LfD need to ensure that the motion trajectories they predict are safe and do not deviate far from the intended goal. Accordingly, the aspect of stability in LfD has received a lot of research focus and many techniques for ensuring stable motions have been proposed. In this paper, we highlight that stable NODEs generated by hypernetworks demonstrate the best empirical performance in learning and remembering multiple LfD skills continually compared to other continual learning approaches (such as dynamic architectures, replay, direct regularization) as well as to hypernetwork-generated NODEs [7] that do not guarantee stability. To aid

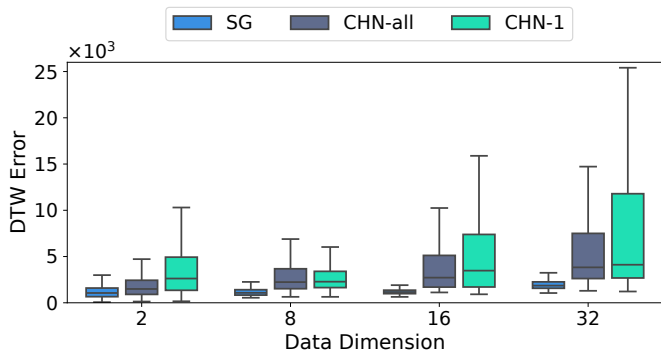


Fig. 21. DTW errors (y-axis) for stochastic regularization in CHN \rightarrow sNODE for all the LASA datasets of different dimensions (x-axis). The upper baseline SG (using sNODE) provides the reference for good performance, but has many more parameters than the CHN models. CHN-1 uses 1 randomly selected task embedding for regularization. CHN-all uses all available task embeddings. CHN-1 performs equivalently to CHN-all for LASA 8D, but shows higher variability in the results compared to CHN-all for the other datasets.

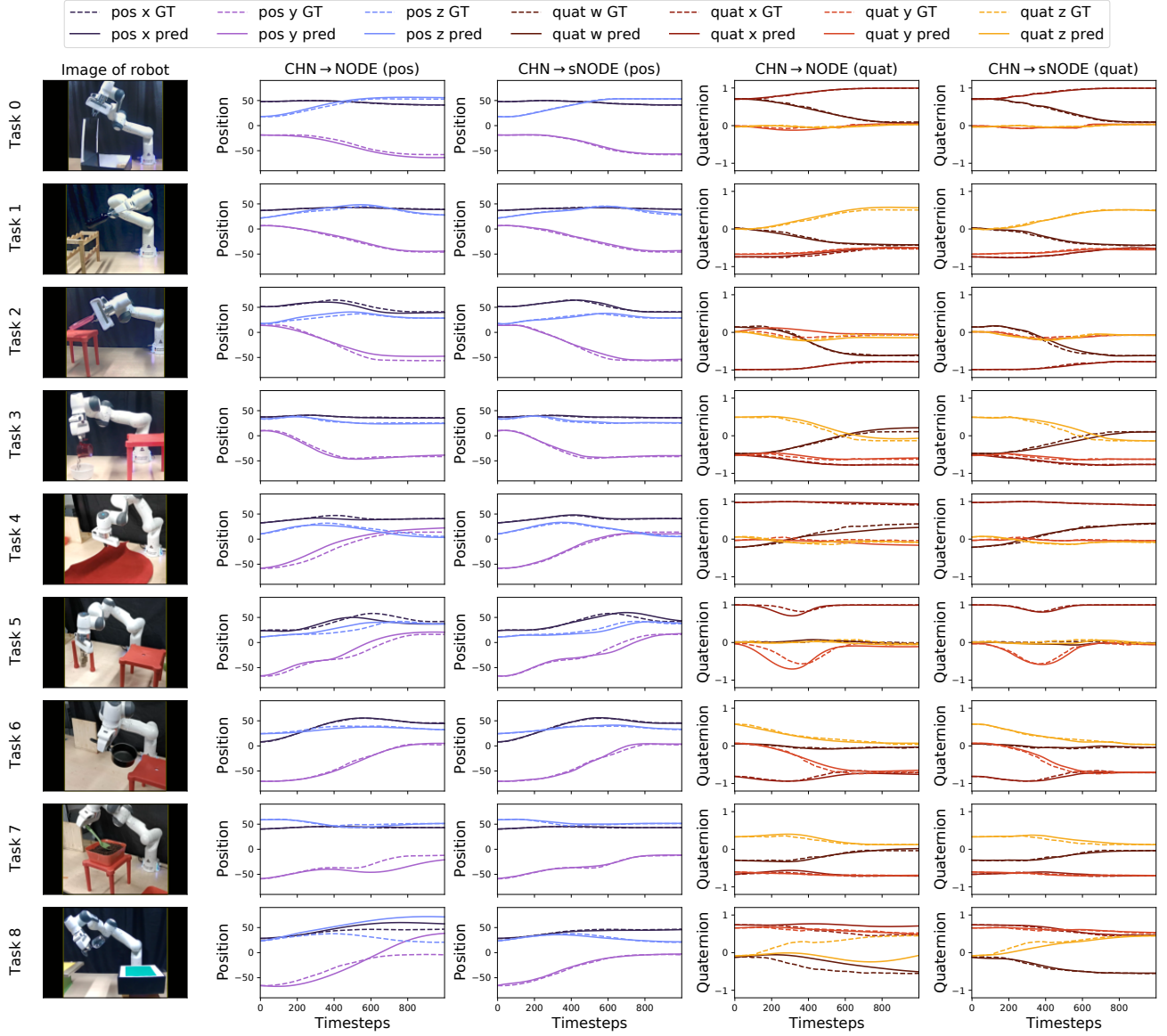


Fig. 22. Qualitative examples for the RoboTasks9 dataset. Models of CHN→NODE and CHN→sNODE are trained sequentially on the 9 tasks of the dataset, and after the last task has been learned, each model is made to perform all the previous tasks. The first column shows images of the robot controlled by CHN→sNODE. The second and third columns show the positions predicted by CHN→NODE and CHN→sNODE respectively. The fourth and fifth columns show the quaternions predicted by CHN→NODE and CHN→sNODE respectively. In the line plots, dotted lines denote the ground truth demonstration and solid lines indicate the predictions. Each row shows a different task. Note the larger errors produced by CHN→NODE compared to CHN→sNODE, particularly for tasks 8, 7, 5, and 4. Videos of the robot performing the tasks from RoboTasks9 can be viewed at <https://youtu.be/xDgTvWADoyA>.

reproducibility and to support further research in continual LfD, our code and datasets are made publicly available.

Across all the datasets ($\mathcal{D}_{\text{LASA2D}}$, $\mathcal{D}_{\text{LASA8D}}$, $\mathcal{D}_{\text{LASA16D}}$, $\mathcal{D}_{\text{LASA32D}}$, \mathcal{D}_{RT9}) that we evaluate on, hypernetwork-generated stable NODE models emerge as the most promising choice empirically for continual-LfD (see sections VI-A, VI-B, and VI-C). Factors such as minimal parameter growth with new tasks, the ability to only use the current data for learning, and their overall continual learning performance make them a robust option for continual LfD. Moreover, we demonstrated that stability within the task learner (i.e. within the sNODE) not only yields stable trajectory predictions but also greatly enhances the overall continual learning performance of hypernetworks. This positive effect is particularly pronounced in the case of smaller,

size-efficient chunked hypernetworks (CHN→sNODE). The constraints of stability can sometimes make learning more difficult and predictions less accurate, but in the case of chunked hypernetworks and sNODE, these constraints instead drive the model to make more efficient use of its limited set of parameters, leading to much improved continual learning performance and the ability to learn and remember a longer sequence of tasks.

Our proposed CHN→sNODE model successfully learns long sequences of 2-dimensional tasks (26 tasks for $\mathcal{D}_{\text{LASA2D}}$, as shown in Fig. 6), scales to high-dimensional trajectories of up to 32 dimensions (as shown in Fig. 13), and learns a long sequence real-world robotic LfD tasks involving trajectories of full 6-DoF poses (for \mathcal{D}_{RT9} , as shown in Fig. 16) only with a

relatively small set of learnable parameters. This positions CHN \rightarrow sNODE as a viable option for continual learning from demonstration on resource-constrained robotic platforms. Additionally, the introduction of stochastic regularization with a single task embedding reduces the time required for training while maintaining overall performance on real-world LfD tasks, enhancing the suitability of hypernetworks for real-world applications.

Future Work: On the high-dimensional LASA 16D and LASA 32D datasets, although our CHN \rightarrow sNODE model is able to remember all tasks and performs better than the non-stable CHN \rightarrow NODE, its performance is still worse than HN \rightarrow sNODE and the upper baseline SG (Fig. 12). Although increasing the chunked hypernetwork parameter size can be a possible solution, an adaptive regularization constant can balance the learning of new tasks against the remembering of old ones in a smarter way. Additionally, for higher-dimensional tasks, future work can also consider tuning important sNODE-specific hyperparameters (such as α in Eq. (4)) for better performance.

Chunked hypernetworks have a fixed capacity: the network does not grow, and storage of task embeddings for each new task results in only a negligible growth of the overall parameter size. As it keeps on learning new tasks, at some point it will be impossible to learn new tasks effectively. A mechanism for graceful forgetting can help in this regard by not considering task embeddings from tasks that are too old or not worth remembering in the regularization process. Furthermore, if the same task is demonstrated again, it is better to identify task similarity and update the corresponding task embedding instead of creating a new one as we currently do. We leave such investigations for future work.

The single task embedding-based stochastic hypernetwork regularization process (CHN-1) proposed by us in this paper performs comparably to a fully regularized hypernetwork and the upper baseline SG for LASA 8D and the RoboTasks9 dataset of real-world LfD tasks (Sec. VI-D). However, it performs sub-optimally when the number of tasks is high (LASA 2D) or when the number of training iterations is insufficient for the complexity of the tasks (LASA 16D and 32D). Instead of sampling the task embeddings uniformly as we do now, in the future we can employ a priority-based sampling procedure to sample task embeddings that are important for maintaining performance on older tasks more frequently than other task embeddings.

Other ways of extending our current work in the future may include devising methods to effectively chain together multiple tasks learned by a CHN/HN model, or to develop a high-level planner that leverages the diverse set of learned tasks as a versatile skill library for more complex applications.

VIII. CONCLUSION

In this paper, we presented an approach for continual learning from demonstration with hypernetwork-generated stable neural-ODEs (sNODE). We compared CL methods from all major families and 2 different trajectory learning approaches for each CL method (NODE and sNODE). We performed a large

number of experiments on 5 different datasets comprising different number of tasks (varying from 9 to 26 tasks), different trajectory dimensions (varying from 2 to 32), and real-world LfD tasks (involving trajectories of full 6-DoF robot poses). We reported trajectory error metrics, continual learning metrics that consider several aspects of performance (such as accuracy, remembering capacity, model size and training time), as well as stability metrics. We found that the stability guarantee provided by sNODE regarding the predicted trajectories not only results in non-divergent trajectories, but also improves the continual learning performance and scalability of our hypernetwork models for high-dimensional trajectories as well as for real-world tasks. These benefits are most pronounced in the size-efficient chunked hypernetworks that achieve the highest overall continual learning score. Additionally, we also demonstrated the effectiveness of stochastic hypernetwork regularization with a single task embedding that enables hypernetworks to scale efficiently in terms of training time on real-world LfD tasks. Overall, our results show that the size efficient CHN \rightarrow sNODE model is the best empirical choice for continual learning from demonstration.

REFERENCES

- [1] H. Ravichandar, A. S. Polydoros, S. Chernova, and A. Billard, "Recent advances in robot learning from demonstration," *Annual review of control, robotics, and autonomous systems*, vol. 3, pp. 297–330, 2020.
- [2] J. Urain, M. Ginesi, D. Tateo, and J. Peters, "Imitationflow: Learning deep stable stochastic dynamic systems by normalizing flows," in *2020 IEEE/RSJ International Conference on Intelligent Robots and Systems (IROS)*. IEEE, 2020, pp. 5231–5237.
- [3] M. Hersch, F. Guenter, S. Calinon, and A. Billard, "Dynamical system modulation for robot learning via kinesthetic demonstrations," *IEEE Transactions on Robotics*, vol. 24, no. 6, pp. 1463–1467, 2008.
- [4] M. Saveriano, "An energy-based approach to ensure the stability of learned dynamical systems," in *IEEE International Conference on Robotics and Automation (ICRA)*, 2020, pp. 4407–4413.
- [5] S. M. Khansari-Zadeh and A. Billard, "Learning control lyapunov function to ensure stability of dynamical system-based robot reaching motions," *Robotics and Autonomous Systems*, vol. 62, no. 6, pp. 752–765, 2014.
- [6] J. Z. Kolter and G. Manek, "Learning stable deep dynamics models," *Advances in Neural Information Processing Systems*, vol. 32, pp. 11 128–11 136, 2019.
- [7] S. Auddy, J. Hollenstein, M. Saveriano, A. Rodríguez-Sánchez, and J. Piater, "Continual learning from demonstration of robotics skills," *Robotics and Autonomous Systems*, vol. 165, p. 104427, 2023. [Online]. Available: <https://www.sciencedirect.com/science/article/pii/S0921889023000660>
- [8] R. T. Chen, Y. Rubanova, J. Bettencourt, and D. Duvenaud, "Neural ordinary differential equations," in *Proceedings of the 32nd International Conference on Neural Information Processing Systems*, 2018, pp. 6572–6583.
- [9] D. Ha, A. M. Dai, and Q. V. Le, "Hypernetworks," in *International Conference on Learning Representations*, 2017. [Online]. Available: <https://openreview.net/forum?id=rkpACe1lx>
- [10] J. von Oswald, C. Henning, J. Sacramento, and B. F. Grewe, "Continual learning with hypernetworks," in *International Conference on Learning Representations (ICLR)*, 2019.
- [11] S. M. Khansari-Zadeh and A. Billard, "Learning stable nonlinear dynamical systems with Gaussian mixture models," *IEEE Transactions on Robotics*, vol. 27, no. 5, pp. 943–957, 2011.
- [12] G. I. Parisi, R. Kemker, J. L. Part, C. Kanan, and S. Wermter, "Continual lifelong learning with neural networks: A review," *Neural Networks*, vol. 113, pp. 54–71, 2019.
- [13] S. Calinon, "Learning from demonstration (programming by demonstration)," *Encyclopedia of robotics*, pp. 1–8, 2018.
- [14] A. Billard, S. Calinon, and R. Dillmann, "Learning from humans," *Springer Handbook of Robotics*, 2nd Ed., 2016.

- [15] B. D. Argall, S. Chernova, M. Veloso, and B. Browning, "A survey of robot learning from demonstration," *Robotics and autonomous systems*, vol. 57, no. 5, pp. 469–483, 2009.
- [16] H. Ravichandar, A. Polydoros, S. Chernova, and A. Billard, "Robot learning from demonstration: A review of recent advances," *Annual Review of Control, Robotics, and Autonomous Systems*, 2019.
- [17] S. R. Ahmadzadeh and S. Chernova, "Trajectory-based skill learning using generalized cylinders," *Frontiers in Robotics and AI*, vol. 5, p. 132, 2018.
- [18] C. Gao, H. Gao, S. Guo, T. Zhang, and F. Chen, "CRIL: Continual robot imitation learning via generative and prediction model," in *2021 IEEE/RSJ International Conference on Intelligent Robots and Systems (IROS)*, 2021, pp. 6747–6754.
- [19] Y. Wu and Y. Demiris, "Towards one shot learning by imitation for humanoid robots," in *2010 IEEE international conference on robotics and automation*. IEEE, 2010, pp. 2889–2894.
- [20] B. D. Argall, B. Browning, and M. M. Veloso, "Teacher feedback to scaffold and refine demonstrated motion primitives on a mobile robot," *Robotics and Autonomous Systems*, vol. 59, no. 3–4, pp. 243–255, 2011.
- [21] P. Englert, N. A. Vien, and M. Toussaint, "Inverse kkt: Learning cost functions of manipulation tasks from demonstrations," *The International Journal of Robotics Research*, vol. 36, no. 13–14, pp. 1474–1488, 2017.
- [22] S. Calinon, P. Kormushev, and D. G. Caldwell, "Compliant skills acquisition and multi-optima policy search with em-based reinforcement learning," *Robotics and Autonomous Systems*, vol. 61, no. 4, pp. 369–379, 2013.
- [23] N. Das, S. Bechtle, T. Davchev, D. Jayaraman, A. Rai, and F. Meier, "Model-based inverse reinforcement learning from visual demonstrations," in *Conference on Robot Learning*. PMLR, 2021, pp. 1930–1942.
- [24] M. Saveriano, F. J. Abu-Dakka, and V. Kyrki, "Learning stable robotic skills on riemannian manifolds," *Robotics and Autonomous Systems*, vol. 169, p. 104510, 2023.
- [25] J. Urain, N. Funk, J. Peters, and G. Chelvatzi, "Se (3)-diffusionfields: Learning smooth cost functions for joint grasp and motion optimization through diffusion," in *2023 IEEE International Conference on Robotics and Automation (ICRA)*. IEEE, 2023, pp. 5923–5930.
- [26] N. B. Figueroa Fernandez and A. Billard, "A physically-consistent bayesian non-parametric mixture model for dynamical system learning," *Proceedings of Machine Learning Research*, 2018.
- [27] A. J. Ijspeert, J. Nakanishi, and S. Schaal, "Movement imitation with nonlinear dynamical systems in humanoid robots," in *International Conference on Robotics and Automation (ICRA)*, 2002, pp. 1398–1403.
- [28] A. A. Rusu, N. C. Rabinowitz, G. Desjardins, H. Soyer, J. Kirkpatrick, K. Kavukcuoglu, R. Pascanu, and R. Hadsell, "Progressive neural networks," *arXiv preprint arXiv:1606.04671*, 2016.
- [29] S.-A. Rebuffi, A. Kolesnikov, G. Sperl, and C. H. Lampert, "icarl: Incremental classifier and representation learning," in *Proceedings of the IEEE Conference on Computer Vision and Pattern Recognition*, 2017, pp. 2001–2010.
- [30] H. Shin, J. K. Lee, J. Kim, and J. Kim, "Continual learning with deep generative replay," in *Proceedings of the 31st International Conference on Neural Information Processing Systems*, 2017, pp. 2994–3003.
- [31] J. Kirkpatrick, R. Pascanu, N. Rabinowitz, J. Veness, G. Desjardins, A. A. Rusu, K. Milan, J. Quan, T. Ramalho, A. Grabska-Barwinska *et al.*, "Overcoming catastrophic forgetting in neural networks," *Proceedings of the national academy of sciences*, vol. 114, no. 13, pp. 3521–3526, 2017.
- [32] F. Zenke, B. Poole, and S. Ganguli, "Continual learning through synaptic intelligence," in *International Conference on Machine Learning*. PMLR, 2017, pp. 3987–3995.
- [33] R. Aljundi, F. Babiloni, M. Elhoseiny, M. Rohrbach, and T. Tuytelaars, "Memory aware synapses: Learning what (not) to forget," in *Proceedings of the European Conference on Computer Vision (ECCV)*, 2018, pp. 139–154.
- [34] M. Delange, R. Aljundi, M. Masana, S. Parisot, X. Jia, A. Leonardis, G. Slabaugh, and T. Tuytelaars, "A continual learning survey: Defying forgetting in classification tasks," *IEEE Transactions on Pattern Analysis and Machine Intelligence*, 2021.
- [35] S. Thrun and T. M. Mitchell, "Lifelong robot learning," *Robotics and Autonomous Systems*, vol. 15, no. 1, pp. 25–46, Jul. 1995.
- [36] N. Churamani, S. Kalkan, and H. Gunes, "Continual Learning for Affective Robotics: Why, What and How?" in *2020 29th IEEE International Conference on Robot and Human Interactive Communication (RO-MAN)*. Naples, Italy: IEEE, Aug. 2020, pp. 425–431.
- [37] N. Churamani, M. Axelsson, A. Çaldir, and H. Gunes, "Continual Learning for Affective Robotics: A Proof of Concept for Wellbeing," in *2022 10th International Conference on Affective Computing and Intelligent Interaction Workshops and Demos (ACIIW)*. Nara, Japan: IEEE, Oct. 2022, pp. 1–8.
- [38] B. Liu, X. Xiao, and P. Stone, "A Lifelong Learning Approach to Mobile Robot Navigation," *IEEE Robotics and Automation Letters*, vol. 6, no. 2, pp. 1090–1096, Apr. 2021. [Online]. Available: <https://ieeexplore.ieee.org/document/9345478/>
- [39] D. Lopez-Paz and M. Ranzato, "Gradient episodic memory for continual learning," *Advances in neural information processing systems*, vol. 30, 2017.
- [40] M. Trinh, J. Moon, L. Grundel, V. Hankemeier, S. Storms, and C. Brecher, "Development of a Framework for Continual Learning in Industrial Robotics," in *2022 IEEE 27th International Conference on Emerging Technologies and Factory Automation (ETFA)*. Stuttgart, Germany: IEEE, Sep. 2022, pp. 1–8. [Online]. Available: <https://ieeexplore.ieee.org/document/9921432/>
- [41] A. Sarabakha, Z. Qiao, S. Ramasamy, and P. N. Suganthan, "Online Continual Learning for Control of Mobile Robots," in *2023 International Joint Conference on Neural Networks (IJCNN)*. Gold Coast, Australia: IEEE, Jun. 2023, pp. 1–10. [Online]. Available: <https://ieeexplore.ieee.org/document/10191188/>
- [42] A. Chaudhry, M. Rohrbach, M. Elhoseiny, T. Ajanthan, P. Dokania, P. Torr, and M. Ranzato, "Continual learning with tiny episodic memories," in *Workshop on Multi-Task and Lifelong Reinforcement Learning*, 2019.
- [43] Z. Li and D. Hoiem, "Learning without forgetting," *IEEE transactions on pattern analysis and machine intelligence*, vol. 40, no. 12, pp. 2935–2947, 2017.
- [44] A. Chaudhry, M. Ranzato, M. Rohrbach, and M. Elhoseiny, "Efficient lifelong learning with a-gem," *arXiv preprint arXiv:1812.00420*, 2018.
- [45] A. Chaudhry, P. K. Dokania, T. Ajanthan, and P. H. Torr, "Riemannian walk for incremental learning: Understanding forgetting and intransigence," in *Proceedings of the European conference on computer vision (ECCV)*, 2018, pp. 532–547.
- [46] Y. Huang, K. Xie, H. Bharadhwaj, and F. Shkurti, "Continual model-based reinforcement learning with hypernetworks," in *2021 IEEE International Conference on Robotics and Automation (ICRA)*. IEEE, 2021, pp. 799–805.
- [47] P. Schöpf, S. Auddy, J. Hollenstein, and A. Rodriguez-Sanchez, "Hypernetwork-ppo for continual reinforcement learning," in *Deep Reinforcement Learning Workshop NeurIPS*, 2022.
- [48] J. Schulman, F. Wolski, P. Dhariwal, A. Radford, and O. Klimov, "Proximal policy optimization algorithms," *arXiv preprint arXiv:1707.06347*, 2017.
- [49] B. Amos, L. Xu, and J. Z. Kolter, "Input convex neural networks," in *International Conference on Machine Learning*. PMLR, 2017, pp. 146–155.
- [50] A. Ude, B. Nemec, T. Petrić, and J. Morimoto, "Orientation in cartesian space dynamic movement primitives," in *2014 IEEE International Conference on Robotics and Automation (ICRA)*. IEEE, 2014, pp. 2997–3004.
- [51] Y. Huang, F. J. Abu-Dakka, J. Silvério, and D. G. Caldwell, "Toward orientation learning and adaptation in cartesian space," *IEEE Transactions on Robotics*, vol. 37, no. 1, pp. 82–98, 2020.
- [52] M. Saveriano, F. Franzel, and D. Lee, "Merging position and orientation motion primitives," in *2019 International Conference on Robotics and Automation (ICRA)*. IEEE, 2019, pp. 7041–7047.
- [53] X. Li, Y. Zhou, T. Wu, R. Socher, and C. Xiong, "Learn to grow: A continual structure learning framework for overcoming catastrophic forgetting," in *International Conference on Machine Learning*. PMLR, 2019, pp. 3925–3934.
- [54] J. Yoon, E. Yang, J. Lee, and S. J. Hwang, "Lifelong learning with dynamically expandable networks," *arXiv preprint arXiv:1708.01547*, 2017.
- [55] J. M. Lee, "Introduction to smooth manifolds." Springer, 2012.
- [56] D. Brahma, V. K. Verma, and P. Rai, "Hypernetworks for continual semi-supervised learning," *arXiv preprint arXiv:2110.01856*, 2021.
- [57] C. Blocher, M. Saveriano, and D. Lee, "Learning stable dynamical systems using contraction theory," in *2017 14th International Conference on Ubiquitous Robots and Ambient Intelligence (URAI)*. IEEE, 2017, pp. 124–129.
- [58] C. F. Jekel, G. Venter, M. P. Venter, N. Stander, and R. T. Haftka, "Similarity measures for identifying material parameters from hysteresis loops using inverse analysis," *International Journal of Material Forming*, vol. 12, no. 3, pp. 355–378, 2019.
- [59] N. Díaz-Rodríguez, V. Lomonaco, D. Filliat, and D. Maltoni, "Don't forget, there is more than forgetting: new metrics for continual learning," *arXiv preprint arXiv:1810.13166*, 2018.

APPENDIX

A. Stable NODE with Time input

We present the benefit of introducing the additional time input to the s NODE model, as described in Sec. IV-A. For this, we train a separate s NODE model on each of the 26 tasks of $\mathcal{D}_{\text{LASA2D}}$. We train two versions of the s NODE model: the original model proposed by [6], which is independent of the time input (we refer to this as s NODE-I), and an s NODE model with our modification of adding the time input (we refer to this as s NODE-T). After learning a task, each model is evaluated on the task it has learned. Each experiment is repeated 5 times with independent seeds. As can be seen in Fig. A.23, s NODE-T produces lower median DTW errors and a smaller variance in performance for all 26 tasks. Accordingly, in this paper, we use s NODE-T in all our experiments and we refer to it simply as s NODE. Also, in our experiments, we use the NODE model with time input (NODE-T) [7]. For this too, we omit the -T ending for brevity.

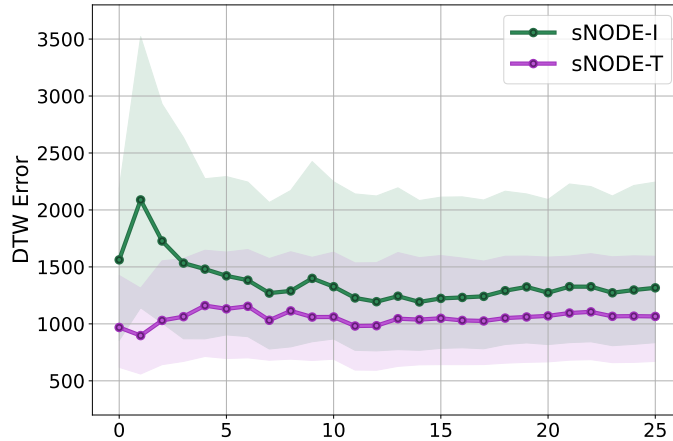


Fig. A.23. Comparison of DTW errors of predictions (lower is better) produced by s NODE with time input (s NODE-T) (ours), and the original s NODE model [6] without any time input (s NODE-I) on the 26 tasks of $\mathcal{D}_{\text{LASA2D}}$. s NODE-T produces lower errors and less variability than s NODE-I for all tasks.

B. LASA 2D - Additional Results

Tab. A.1 presents the continual learning metrics for the different CL methods using NODE or s NODE as the task learner on the LASA 2D dataset. s NODE improves the continual learning performance of REP, HN and particularly that of CHN (compare the entries in Tab. A.1(a) to the corresponding entry in Tab. A.1(b)). Each continual learning metric ranges from 0 (worst) to 1 (best). The overall continual learning performance is represented by the CL_{score} column.

MET	ACC	REM	MS	TE	FS	SSS	CL_{sco}	CL_{stab}	MET	ACC	REM	MS	TE	FS	SSS	CL_{sco}	CL_{stab}
SG	0.89	1.00	0.15	0.99	0.00	1.00	0.67	0.53	SG	0.87	1.00	0.15	0.99	0.00	1.00	0.67	0.54
FT	0.06	0.19	1.00	0.99	0.96	1.00	0.70	0.55	FT	0.06	0.20	1.00	0.98	0.95	1.00	0.70	0.56
REP	0.56	1.00	1.00	0.99	0.96	0.48	0.83	0.76	REP	0.73	1.00	1.00	0.99	0.95	0.48	0.86	0.79
SI	0.05	0.36	1.00	0.92	0.78	1.00	0.68	0.61	SI	0.02	0.53	1.00	0.97	0.75	1.00	0.71	0.62
MAS	0.01	0.87	1.00	0.89	0.83	1.00	0.76	0.62	MAS	0.08	0.38	1.00	0.86	0.80	1.00	0.69	0.63
HN	0.80	0.96	1.00	0.46	0.90	1.00	0.85	0.79	HN	0.88	0.98	1.00	0.71	0.88	1.00	0.91	0.89
CHN	0.39	0.72	1.00	0.45	0.96	1.00	0.75	0.72	CHN	0.70	0.90	1.00	0.71	0.96	1.00	0.88	0.86

(a) NODE

(b) s NODE

TABLE A.1

CONTINUAL LEARNING METRICS FOR THE LASA 2D DATASET (MEDIAN OVER 5 SEEDS). VALUES RANGE FROM 0 (WORST) TO 1 (BEST). $\text{HN} \rightarrow s\text{NODE}$, FOLLOWED BY $\text{CHN} \rightarrow s\text{NODE}$ ACHIEVE THE BEST OVERALL CONTINUAL LEARNING SCORE AMONGST ALL METHODS.

C. High-dimensional LASA - Additional Results

Continual learning metrics (0:worst-1:best) for SG, FT, REP, HN, and CHN for the high-dimensional LASA 8D dataset are presented in Tab. A.2. The scores for both task learners (NODE and s NODE) are shown. The use of s NODE improves the continual learning performance of $\text{CHN} \rightarrow s\text{NODE}$, which achieves the best overall continual learning performance among all methods. CL metrics for LASA 16D and LASA 32D are shown in Tab. A.3 and Tab. A.4 respectively. For both these datasets, $\text{HN} \rightarrow s\text{NODE}$ and $\text{CHN} \rightarrow s\text{NODE}$ obtain the best CL scores among all methods (across s NODE and NODE). For computing the CL metrics, DTW threshold values of 4000, 7000 and 15000 were set empirically for $\mathcal{D}_{\text{LASA8D}}$, $\mathcal{D}_{\text{LASA16D}}$, and $\mathcal{D}_{\text{LASA32D}}$ respectively. In Fig. A.24, we present the DTW errors evaluated after each task is learned while training on the

MET	ACC	REM	MS	TE	FS	SSS	CL _{sco}	CL _{stab}
SG	0.96	1.00	0.29	1.00	0.00	1.00	0.71	0.55
FT	0.18	0.06	1.00	1.00	0.89	1.00	0.69	0.56
REP	0.56	0.98	1.00	1.00	0.89	0.45	0.81	0.76
HN	0.83	0.99	1.00	0.64	0.62	1.00	0.85	0.82
CHN	0.52	0.98	1.00	0.65	0.82	1.00	0.83	0.80

(a) LASA 8D NODE

MET	ACC	REM	MS	TE	FS	SSS	CL _{sco}	CL _{stab}
SG	1.00	1.00	0.29	1.00	0.00	1.00	0.72	0.55
FT	0.18	0.04	1.00	0.99	0.84	1.00	0.68	0.55
REP	0.69	1.00	1.00	0.99	0.84	0.45	0.83	0.78
HN	0.94	0.99	1.00	0.87	0.49	1.00	0.88	0.80
CHN	0.79	0.99	1.00	0.84	0.77	1.00	0.90	0.89

(b) LASA 8D sNODE

TABLE A.2

CONTINUAL LEARNING METRICS FOR THE HIGH-DIMENSIONAL LASA 8D DATASET (MEDIAN OVER 5 SEEDS). VALUES RANGE FROM 0 (WORST) TO 1 (BEST).

MET	ACC	REM	MS	TE	FS	SSS	CL _{sco}	CL _{stab}
SG	1.00	1.00	0.29	1.00	0.00	1.00	0.72	0.55
FT	0.18	0.00	1.00	1.00	0.89	1.00	0.68	0.54
REP	0.82	1.00	1.00	0.99	0.89	0.45	0.86	0.79
HN	0.93	0.99	1.00	0.64	0.62	1.00	0.86	0.82
CHN	0.82	1.00	1.00	0.59	0.87	1.00	0.88	0.84

(a) LASA 16D NODE

MET	ACC	REM	MS	TE	FS	SSS	CL _{sco}	CL _{stab}
SG	1.00	1.00	0.29	0.99	0.00	1.00	0.71	0.55
FT	0.18	0.00	1.00	0.99	0.89	1.00	0.68	0.54
REP	0.80	1.00	1.00	0.99	0.89	0.45	0.85	0.79
HN	0.99	1.00	1.00	0.84	0.70	1.00	0.92	0.88
CHN	0.85	1.00	1.00	0.82	0.87	1.00	0.92	0.91

(b) LASA 16D sNODE

TABLE A.3

CONTINUAL LEARNING METRICS FOR THE HIGH-DIMENSIONAL LASA 16D DATASET (MEDIAN OVER 5 SEEDS). VALUES RANGE FROM 0 (WORST) TO 1 (BEST).

MET	ACC	REM	MS	TE	FS	SSS	CL _{sco}	CL _{stab}
SG	1.00	1.00	0.29	1.00	0.00	1.00	0.71	0.55
FT	0.18	0.00	1.00	0.98	0.89	1.00	0.68	0.54
REP	0.85	1.00	1.00	0.99	0.89	0.45	0.86	0.79
HN	0.99	1.00	1.00	0.64	0.72	1.00	0.89	0.83
CHN	0.82	0.99	1.00	0.57	0.87	1.00	0.88	0.83

(a) LASA 32D NODE

MET	ACC	REM	MS	TE	FS	SSS	CL _{sco}	CL _{stab}
SG	1.00	1.00	0.29	1.00	0.00	1.00	0.72	0.55
FT	0.18	0.01	1.00	0.99	0.88	1.00	0.68	0.55
REP	0.84	1.00	1.00	0.99	0.88	0.45	0.86	0.79
HN	0.99	1.00	1.00	0.84	0.72	1.00	0.92	0.88
CHN	0.93	1.00	1.00	0.77	0.87	1.00	0.93	0.91

(b) LASA 32D sNODE

TABLE A.4

CONTINUAL LEARNING METRICS FOR THE HIGH-DIMENSIONAL LASA 32D DATASET (MEDIAN OVER 5 SEEDS). VALUES RANGE FROM 0 (WORST) TO 1 (BEST).

high-dimensional LASA datasets, where CHN→sNODE shows better performance than CHN→NODE overall. In Fig. A.25, we show qualitative examples of predictions made by CHN→NODE (shows divergence) and CHN→sNODE (shows no divergence) for the LASA 8D dataset.

D. RoboTasks9 - Additional Results

We present the complete set of results for the evaluation of continual learning metrics for the RoboTasks9 dataset in Tab. A.5 (CL metrics based on the positional DTW errors) and Tab. A.6 (CL metrics based on the orientation errors). The use of sNODE over NODE improves the continual learning performance of REP, HN and particularly that of CHN, which achieves the best overall continual learning performance for both position and orientation among all methods.

E. Hyperparameters

In Tab. A.7, we present the complete set of hyperparameters used in our experiments. For experiments on the LASA 2D datasets, we use the same hyperparameters as [7]. For LASA 8D and RoboTasks9, we scale the number of training iterations roughly proportional to the dimension of the trajectories in the respective datasets. For LASA 16D and LASA 32D, we use much fewer iterations than what the linear scaling based on data dimension would suggest to keep the overall runtime of the large number experiments we perform within bounds. Since sNODE contains an extra network for the parameterized Lyapunov function, the architecture of the NODE and sNODE models are adjusted (layers contain different number of neurons) so that the final parameter count of a NODE model and the corresponding sNODE model is roughly the same.

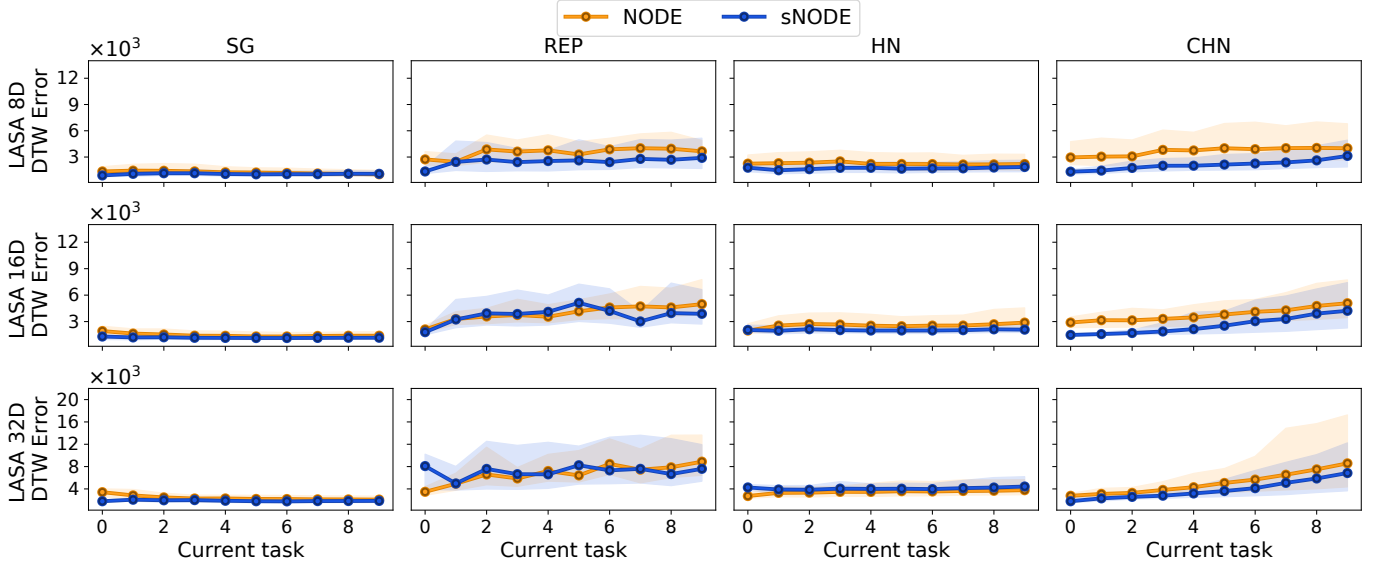


Fig. A.24. DTW errors of SG, REP, HN, and CHN for the high-dimensional LASA datasets (lower is better). The x-axis shows the current task. After learning each new task, the current and all previous tasks are evaluated. The DTW errors of these predictions are shown on the y-axis. Lines show the medians and the shaded region represents the inter-quartile range of results for 5 independent seeds. The performance of SG with NODE and sNODE is equivalent and there are minor improvements for HN with an sNODE. CHN→sNODE is able to remember all tasks and produces lower median errors than CHN→NODE and with lower variability in the results. The first, second and third rows show the results for LASA 8D, 16D and 32D respectively.

F. Stability Tests

For testing the stability of the trajectories predicted by our proposed continual-LfD models for the LASA 2D dataset, we initialize trained models of CHN→NODE and CHN→sNODE (after learning the 26 tasks of the dataset) with starting positions that are different from the ground truth demonstrations. For each model, and for each past task, we choose a 100 random starting positions by uniformly sampling points that lie within a circle of radius 25 cm around the ground truth start position. The CHN→NODE and CHN→sNODE models then predict trajectories for each of these start positions. Qualitative examples of these predicted trajectories for a couple of tasks were presented earlier in Fig. 11. We perform quantitative evaluation of this test as well. For each random start position, we measure the *End position* Δ , i.e. the distance of the final point of the predicted trajectory from the ground truth goal, presented in Fig. A.26, that shows that CHN→NODE produces highly divergent trajectories for multiple tasks, while CHN→sNODE does not, leading to much lower values of *End position* Δ for CHN→sNODE compared to CHN→NODE. We perform this test on the LASA 2D dataset because the high number of tasks in this dataset allows us to test the convergence/divergence of the predictions for a large variety of trajectory shapes and start positions.

Additionally, we also evaluate how stable the models are near the goal. The ground truth demonstrations used for training the models are of 1000 steps. During inference, after the trajectory predicted by a model reaches the goal (or sufficiently close to the goal), it should not deviate away from the goal. To test this, we take the models that are trained on 1000 step demonstrations and make them predict trajectories of 1100 and 1200 steps. We perform this evaluation for the LASA 2D and RoboTasks9 datasets, and repeat each evaluation 5 times with independent seeds. For each predicted trajectory, we measure the distance of the final point of the predicted trajectory and the goal (i.e. the final point of the ground truth demonstration). As shown in Fig. A.27 and Fig. A.28, for multiple tasks CHN→NODE is unable to stay at the goal which results in higher distances to

MET	ACC	REM	MS	TE	FS	SSS	CL _{sco}	CL _{stab}
SG	0.87	1.00	0.31	1.00	0.00	1.00	0.70	0.57
FT	0.16	0.16	1.00	1.00	0.87	1.00	0.70	0.58
REP	0.60	0.96	1.00	0.99	0.87	0.44	0.81	0.77
HN	0.76	1.00	1.00	0.68	0.54	1.00	0.83	0.80
CHN	0.53	0.95	1.00	0.70	0.84	1.00	0.84	0.81

(a) NODE

MET	ACC	REM	MS	TE	FS	SSS	CL _{sco}	CL _{stab}
SG	0.88	1.00	0.31	0.99	0.00	1.00	0.70	0.57
FT	0.17	0.08	1.00	0.98	0.86	1.00	0.68	0.57
REP	0.80	1.00	1.00	0.98	0.86	0.44	0.85	0.79
HN	0.85	0.99	1.00	0.86	0.44	1.00	0.86	0.78
CHN	0.73	0.97	1.00	0.87	0.84	1.00	0.90	0.89

(b) sNODE

TABLE A.5

CONTINUAL LEARNING METRICS FOR THE POSITION TRAJECTORIES OF THE ROBOTASKS DATASET (MEDIAN OVER 5 SEEDS). VALUES RANGE FROM 0 (WORST) TO 1 (BEST).

MET	ACC	REM	MS	TE	FS	SSS	CL _{sco}	CL _{stab}
SG	0.90	1.00	0.31	1.00	0.00	1.00	0.70	0.56
FT	0.17	0.14	1.00	1.00	0.87	1.00	0.70	0.58
REP	0.74	0.97	1.00	0.99	0.87	0.44	0.84	0.78
HN	0.78	1.00	1.00	0.68	0.54	1.00	0.83	0.80
CHN	0.69	0.90	1.00	0.70	0.84	1.00	0.86	0.86

(a) NODE

MET	ACC	REM	MS	TE	FS	SSS	CL _{sco}	CL _{stab}
SG	0.96	1.00	0.31	0.99	0.00	1.00	0.71	0.56
FT	0.20	0.01	1.00	0.98	0.86	1.00	0.67	0.55
REP	0.92	1.00	1.00	0.98	0.86	0.44	0.87	0.79
HN	0.92	0.99	1.00	0.86	0.44	1.00	0.87	0.78
CHN	0.86	0.98	1.00	0.87	0.84	1.00	0.92	0.92

(b) sNODE

TABLE A.6

CONTINUAL LEARNING METRICS FOR THE ORIENTATION TRAJECTORIES OF THE RoboTasks DATASET (MEDIAN OVER 5 SEEDS). VALUES RANGE FROM 0 (WORST) TO 1 (BEST).

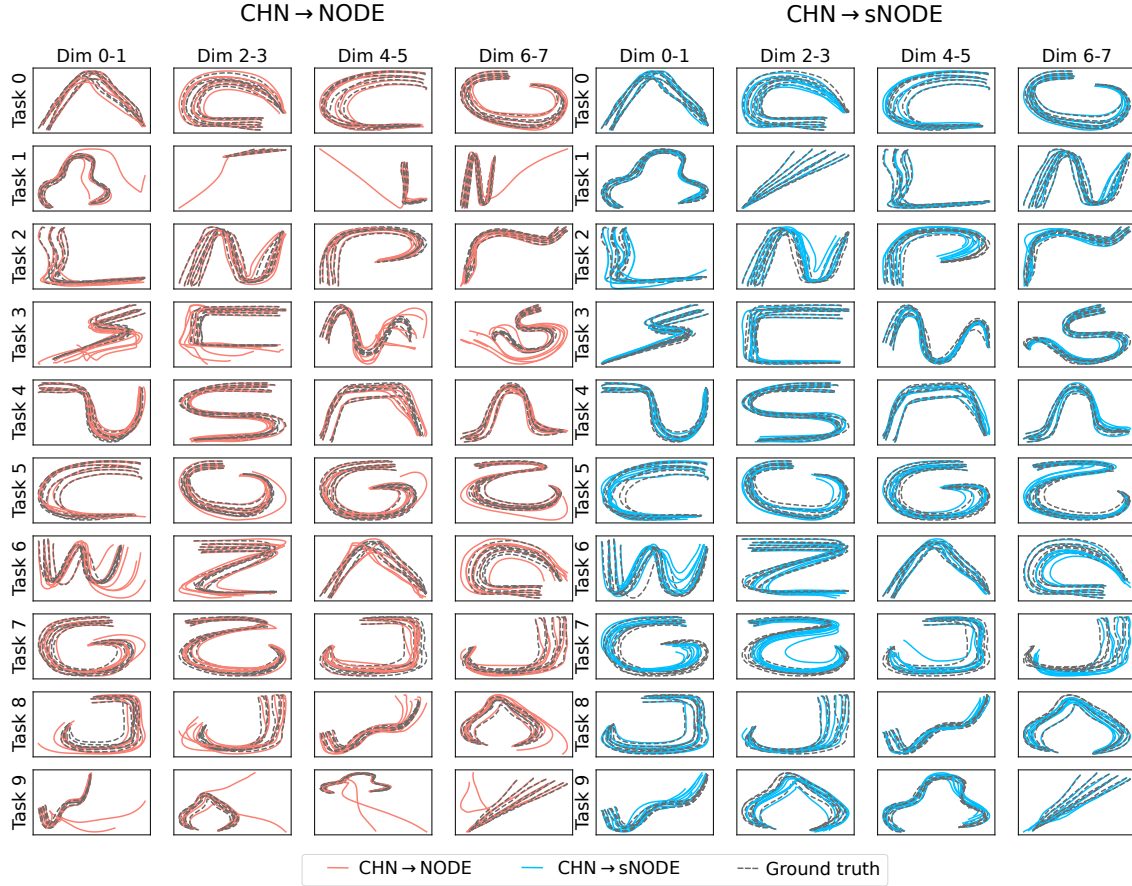


Fig. A.25. Qualitative examples of predictions produced by (a) CHN→NODE and (b) CHN→sNODE for the 10 tasks of the LASA 8D dataset after learning all tasks. The ground truth is shown with grey dotted lines, the predictions of CHN→NODE with orange lines and the predictions of CHN→sNODE with blue lines. Each row represents a single task. Each column shows 2 consecutive dimensions of the 8-dimensional task. The first set of 4 columns show CHN→NODE and the last 4 columns show CHN→sNODE. Overall, CHN→sNODE does not show divergence and produces much fewer erroneous predictions than CHN→NODE.

the ground truth goal for 100 and 200 extra steps. CHN→sNODE on the other hand, shows much more stable behavior and remains close to the goal irrespective of the number of extra steps for both the LASA 2D and RoboTasks9 datasets.

Dataset	LASA 2D	LASA 8D	LASA 16D	LASA 32D	RoboTasks9
Dimension	2	8	16	32	6
Iterations	1.5×10^4	6.0×10^4	7.0×10^4	8.0×10^4	4.0×10^4
LR	1.0×10^{-4}	5.0×10^{-5}	5.0×10^{-5}	5.0×10^{-5}	5.0×10^{-5}
SI C	0.3	-	-	-	-
SI ϵ	0.3	-	-	-	-
MAS λ	0.1	-	-	-	-
arch(NODE)	[1000]x2, 1015	[1000]x3, 1015	[1000]x4, 1015	[1000]x5, 1015	[1000]x2, 1015
arch(s NODE \hat{f})	[1000]x3	[1000]x3	[1000]x3	[1000]x3	[1000]x3
arch(s NODE V)	[100]x2	[100]x2	[100]x2	[100]x2	[100]x2
arch(HN NODE)	[100]x2, 150	[100]x3, 150	[100]x4, 150	[80]x5, 100	[100]x2, 150
arch(HN s NODE \hat{f})	[100]x3	[90]x3	[75]x3	[60]x3	[100]x3
arch(HN/CHN)	[200]x3	[300]x3	[300]x3	[350]x3	[300]x3
dim(Task Emb)	256	256	256	512	256
HN/CHN β	5.0×10^{-3}	5.0×10^{-3}	5.0×10^{-3}	5.0×10^{-3}	5.0×10^{-3}
dim(CHN Chunk Emb)	256	256	256	512	256
dim(CHN Chunk)	8192	16384	16384	16384	8192
Tangent vector scale	-	-	-	-	5.0

TABLE A.7

HYPERPARAMETERS USED IN OUR EXPERIMENTS. THE SAME NODE AND s NODE ARCHITECTURES ARE USED FOR SG, REP, FT, SI, MAS AND CHN. SMALLER NETWORKS FOR NODE AND s NODE ARE USED FOR HN TO KEEP THE HYPERNETWORK SIZE COMPARABLE. TANGENT VECTOR SCALE IS USED ONLY WHEN ORIENTATIONS ARE LEARNED FOR THE RoboTasks9 DATASET.

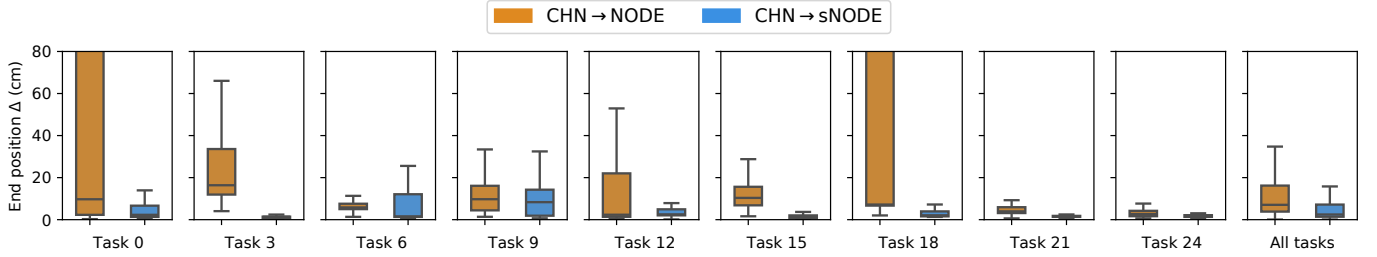


Fig. A.26. Quantitative results of the stability test of CHN→NODE and CHN→ s NODE on $\mathcal{D}_{\text{LASA2D}}$. For each task, the starting position is set randomly from a circle of radius 25 cm around the ground truth starting position, and we measure the distance between the ground truth goal and the end point of the predicted trajectory (goal Δ). (a) CHN→NODE shows divergence for multiple tasks, but CHN→ s NODE converges near or at the goal.

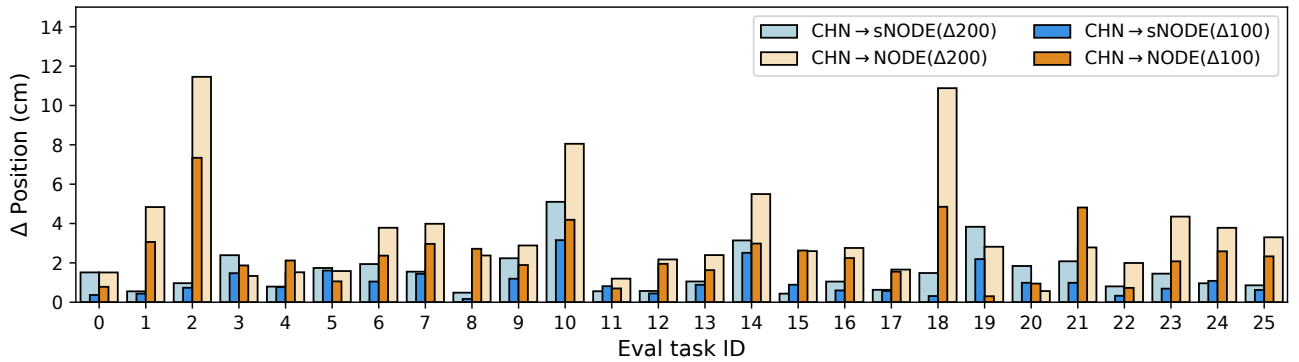


Fig. A.27. On the LASA 2D dataset, we make CHN→NODE and CHN→ s NODE predict trajectories of 1100 and 1200 steps (the models were trained on ground truth demonstrations of 1000 steps) and we measure goal Δ , that is the distance between the ground truth goal and the end point of the predicted trajectories. For many tasks, the goal Δ for CHN→ s NODE is much lower than CHN→NODE.

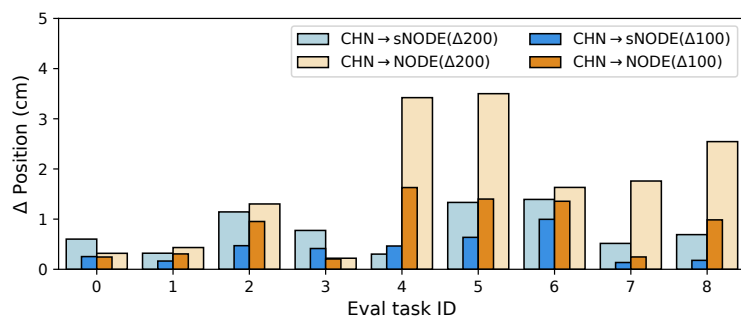


Fig. A.28. On the RoboTasks9 dataset, we make CHN→NODE and CHN→sNODE predict trajectories of 1100 and 1200 steps (the models were trained on ground truth demonstrations of 1000 steps) and we measure goal Δ , that is the distance between the ground truth goal and the end point of the predicted trajectories. For many tasks, the goal Δ for CHN→sNODE is much lower than CHN→NODE.